

Please cite the Published Version

Paparao, Jami, Bhopatrao, Siddharth, Murugan, S and Kuti, Olawole Abiola  (2023) Optimization of a low heat rejection engine run on oxy-hydrogen gas with a biodiesel-diesel blend. Fuel Processing Technology, 241. p. 107625. ISSN 0378-3820

DOI: <https://doi.org/10.1016/j.fuproc.2022.107625>

Publisher: Elsevier

Version: Accepted Version

Downloaded from: <https://e-space.mmu.ac.uk/631200/>

Usage rights:  [Creative Commons: Attribution-Noncommercial-No Derivative Works 4.0](https://creativecommons.org/licenses/by-nc-nd/4.0/)

Additional Information: This is an Accepted Manuscript of an article which appeared in Fuel Processing Technology, published by Elsevier

Enquiries:

If you have questions about this document, contact openresearch@mmu.ac.uk. Please include the URL of the record in e-space. If you believe that your, or a third party's rights have been compromised through this document please see our Take Down policy (available from <https://www.mmu.ac.uk/library/using-the-library/policies-and-guidelines>)

Optimization of a low heat rejection engine run on oxy-hydrogen gas with a biodiesel-diesel blend

Jami Paparao^{a,*}, Siddharth Bhopatrao^a, S. Murugan^a, Olawole Abiola Kuti^b

^a Department of Mechanical Engineering, National Institute of Technology Rourkela, India

^b Department of Mechanical Engineering, The Manchester Metropolitan University, United Kingdom

ABSTRACT

This experimental investigation examines the combined effects of varying compression ratio (CR) and fuel injection parameters such as fuel injection pressure (FIP) and start of injection (SOI) / injection timing on the performance of a dual-fuel low heat rejection (LHR) engine run on oxy-hydrogen (HHO) gas with Jatropa biodiesel-diesel blend (JME20) as pilot fuel. The CR is varied from 16.5 to 18.5 in intervals of one, FIP is varied from 220 to 240 bar in intervals of 20 bar, and the SOI is varied from 24.5° to 27.5° CA bTDC in intervals of 1.5° CA. The performance, emission, and combustion characteristics of the dual-fueled LHR engine are studied, based on which the engine operating conditions are optimized. The results reveal that operating the LHR engine with 18.5 CR, 240 bar FIP, and 26° CA bTDC SOI using HHO in dual fuel operation mode with JME20 injected fuel gives better brake thermal efficiency (BTE) (6.6% higher than diesel) and combustion characteristics along with lower carbon monoxide (CO), hydrocarbon (HC), and smoke emissions. In contrast, a slight penalty in nitric oxide (NO) emissions is noticed irrespective of the engine operating conditions.

1. Introduction

In 2019, about 84% of the primary energy generated from coal, oil, and gas was consumed for electrical power generation, transportation, and heating applications [1]. The transportation sector utilizes about 54.9% of the total global oil reserves [2]. The diesel engine market is envisaged to grow at a compounded annual growth rate (CAGR) of 3.37% from 2019 to 2026 [3]. Diesel engine technology is a well-established technology worldwide. The widespread use of diesel fuel has increased its global demand and also contributed to harmful higher emission levels. It has been estimated that increase in global average temperature beyond 2 °C will cost lives of the millions, and hence an agreement was made at 2015 United Nations Climate Change Conference to limit the global warming below 2 °C [4,5]. Due to these concerns, several governments worldwide are considering strategies to deploy clean and green fuels in compression ignition (CI) engines.

In recent years, the adoption of dual-fuel technology for CI engine applications has been found attractive since, it uses gaseous fuels like LPG, CNG, biogas, and hydrogen as primary fuels which can offer reduced emissions than single fuel operation [6]. Hydrogen is considered to be a better fuel as it has many merits over the other the gaseous

fuels. According to the report of International Energy Agency, hydrogen plays a vital role in Net Zero Emissions by 2050 roadmap and sustainable development [7]. However, despite having remarkable combustion characteristics, there are problems with its storage and large-scale production. Being flammable and explosive, its leakage can have disastrous consequences [8]. Hence, other alternatives that can be produced on-board vehicles and in decentralized diesel power plant locations must be explored. A mixture of hydrogen-oxygen gas also known as HHO gas or Brown gas is an alternative to hydrogen which can be used for CI engine applications [9]. In 1977, Yull Brown patented an electrolytic cell configuration used to produce hydrogen and oxygen in a stoichiometric proportion for welding and brazing applications [10]. HHO gas as fuel contains 2 mol of hydrogen (H₂) and 1 mol of oxygen (O₂). Due to the presence of H₂, it exhibits similar combustion properties as that of hydrogen [11]. It has a higher combustion efficiency than hydrogen because of the presence of O₂. It can be generated by different methods such as electrolysis, thermochemical process, photodialysis, and thermal decomposition of water. Several researchers have used the electrolysis process to generate HHO gas as the method is comparatively efficient, cheap, and promising. Different types of electrolyzers can be used to produce HHO gas from the electrolysis process i.e. dry cell electrolyzer and wet cell electrolyzer. Various research works on the production of

Nomenclature

Abbreviations

APS	Atmospheric Plasma Spray
BP	Brake Power
BSEC	Brake Specific Energy Consumption
BSFC	Brake Specific Fuel Consumption
bTDC	Before Top Dead Centre
BTE	Brake Thermal Efficiency
CAGR	Compounded Annual Growth Rate
CBDA	Chhattisgarh Biodiesel Development Authority
CI	Compression Ignition
CNG	Compressed Natural Gas
CO	Carbon Monoxide
CO ₂	Carbon Dioxide
CR	Compression Ratio
CSIR	Council of Scientific and Industrial Research
D100	Neat Diesel
DAS	Data Acquisition System
DC	Direct Current
DFM	Dual Fuel Mode
DI	Direct Injection
EGR	Exhaust Gas Recirculation
EGT	Exhaust Gas Temperature
FFA	Free Fatty Acid
FIP	Fuel Injection Pressure
HC	Unburnt Hydrocarbon
HCl	Hydrochloric Acid
HHO	Oxy-Hydrogen Gas
ID	Ignition Delay
IMMT	Institute of Minerals and Materials Technology
JME	Jatropha Methyl Ester
JME20	20% JME + 80% Diesel
KOH	Potassium Hydroxide
LHR	Low Heat rejection
LNT	Lean NO _x Trap
LPG	Liquefied Petroleum Gas
LPM	Litres Per Minute
NDIR	Non-Dispersive Infrared

NO	Nitric Oxide
NO ₂	Nitrogen Dioxide
NO _x	Nitrogen Oxides
ppm	Parts Per Million
rpm	Revolutions Per Minute
SCR	Selective Catalytic Reduction
SCRF	SCR Filter
SOI	Start of Injection / Injection timing
SOC	Start of Combustion
NIT	National Institute of Technology
TBC	Thermal Barrier Coating
TDC	Top Dead Centre
YSZ	Yttria Stabilized Zirconia
YSZ + CeO ₂	YSZ + Cerium oxide

Symbols

D	Bore diameter of cylinder
h_{CG}	Clearance height without gasket
L	Stroke length
P	Instantaneous in-cylinder pressure
P_{Max}	Peak in-cylinder pressure
Q_n	Apparent net heat release rate
R	Universal gas constant
T	Instantaneous in-cylinder temperature
T_{MG_1}	Thickness of metal gasket ₁
V	Instantaneous in-cylinder volume
V_{C_1}	Clearance volume ₁
V_{CG}	Clearance volume without gasket
V_{MG_1}	Volume of metal gasket ₁
V_S	Swept volume
X_m	Mean deviation
°CA	Degree Crank Angle

Greek symbols

ΔR	Dependent variable
ΔX_i	Independent variable
γ	Specific heat ratio
σ	Standard deviation

HHO by dry and wet cell generators have been studied and discussed in an earlier review article [11].

Kamaraj et al. [12] examined the effects of inducting 10% HHO on CI engine behavior and reported that fuel consumption decreased by around 11.8%, while brake thermal efficiency (BTE) increased by 4.9%. Unburnt hydrocarbon (HC), carbon monoxide (CO), and smoke emissions were lower by 22.2%, 6.3%, and 11.4%, respectively, at 75% load but carbon dioxide (CO₂) and nitrogen oxides (NO_x) were higher by 3.4% and 22.4% respectively. The improvements were due to higher energy content and complete combustion of hydrogen. Although the use of diesel with HHO in dual-fuel mode (DFM) results in superior engine performance, NO_x emissions are higher when compared to those of neat diesel. Suja and Nagarajan [13] attempted to reduce NO_x emissions of a dual-fuel CI engine run on HHO as the primary fuel to neat diesel level by exhaust gas recirculation (EGR). The authors reported that a 2.44% reduction in NO_x emissions when the engine was operated at 50% load. Pathak et al. [14] also observed a similar trend while reducing NO_x emissions using CNG-diesel in DFM with the EGR technique.

To reduce the dependency on diesel as a pilot fuel, researchers examined the utilization of biodiesel and diesel blends as a pilot fuel along with HHO in DFM operation [15]. Rahman et al. [16] did a comparative study on HHO and hydrogen induction along with algal biodiesel (B40) as pilot fuel in DFM. The HHO + B40 operation gave a

6.5% increase in BTE and a 7.14% reduction in Brake specific fuel consumption (BSFC) in comparison with hydrogen+B40. This was due to the supplementary oxygen provided by HHO which promoted complete combustion. Daniel et al. [15] used Karanja and microalgae biodiesel blend (KOME5MCP5) as pilot fuel in a HHO dual-fuel engine and observed a 9.73% and 6.98% increase in the heat release rate (HRR) and cylinder pressure respectively at full load. Although biodiesel has a lower calorific value than diesel and hydrogen, the higher flame velocity and higher calorific value of HHO help to improve the combustion process. Baltacioglu et al. [17] investigated the effect of the consumption of 1 l per minute (LPM) of HHO gas along with a diesel-biodiesel-ethanol blend as a pilot fuel in DFM. They reported about 12.2% average CO reduction in the operation. This was attributed to the carbon-free nature of HHO as well as the complete combustion promoted by HHO. However, the high combustion temperature produced by HHO resulted in an average increase of thermal NO_x by 9.47%. Najafi et al. examined various blends (B0, B5, B20) of waste cooking oil-biodiesel as pilot fuels with the induction of HHO gas at various flow rates (3, 4, and 5 cc/s) in DFM. The induction of HHO at a flow rate of 5 cc/s with B20 as injected fuel resulted in the highest exhaust gas temperature (EGT) because of the oxygen in biodiesel as well as HHO. Higher combustion efficiency of HHO also caused higher EGT [18]. Sekar et al. [19] used HHO gas along with an orange peel-biodiesel

blend (O25/O50) in DFM for operating a CI engine. The engine exhibited better performance and lower emissions compared to other blends due to the presence of oxygen in both biodiesel and HHO, which enhanced the combustion process.

The selection of pilot fuel in DFM also plays a key role in the performance of the CI engine. Biodiesel is one of the suitable alternative fuels for diesel which has potential to meet the current sustainability goals [20]. The presence of oxygen in biodiesel [21] significantly reduces particulate matter (PM) emissions and contributes towards better combustion characteristics [22,23]. The higher viscosity of biodiesel may lead to improper mixing of air-fuel but at the same time it lowers the phenomenon of engine blow-by [24]. A lot of research works are available on the use of different biodiesels in CI engine applications. Among the different biodiesels examined, Jatropha biodiesel is considered as a potential fuel in tropical and sub-tropical regions because of its easy production. Research works have proved that among various Jatropha methyl ester (JME) and its diesel blends as fuels, a blend containing 20% JME and 80% diesel (JME20) gives superior performance and comparable emissions to those of the dual-fuel operation. Therefore, JME20 has been used as pilot fuel in the present research work.

1.1. Novelty and objective of research work

Many research works are available on the use of HHO gas along with diesel or biodiesel as pilot fuels in CI engines, but there are only a few studies on the use of HHO gas in LHR engines. To the best of the authors' knowledge, there are no research studies available on the optimization of the HHO dual-fueled LHR engine thus far. Based on this perceived research gap, a set of (3³) experiments are conducted by varying the engine input operating conditions such as compression ratio (CR), fuel injection pressure (FIP), and the start of injection (SOI)/injection timing of a LHR engine run on HHO gas with JME20 in DFM for determining the optimized LHR engine conditions to augment performance and minimize the emissions.

2. Materials and methods

2.1. Test fuel modification

2.1.1. HHO gas

Fig. 1 displays the schematic layout of the HHO gas production generator. In this research work, a lab scale (0.75 LPM) wet cell HHO gas generator is developed in the Heat and Power laboratory of the National Institute of Technology (NIT), Rourkela. Table 1 lists some important properties of different gaseous fuels.

2.1.2. Biodiesel-diesel blend (JME20)

The Chhattisgarh Biodiesel Development Authority (CBDA), Raipur,

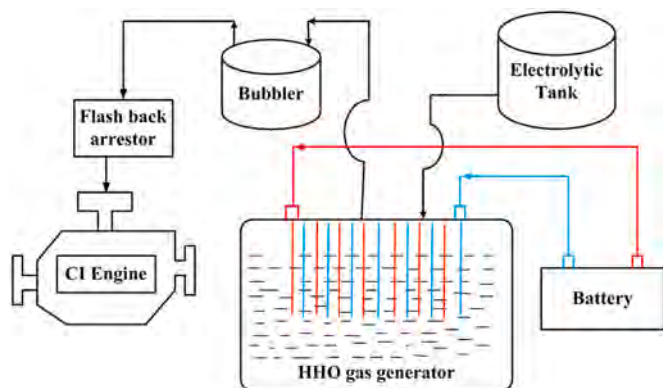


Fig. 1. Wet cell HHO gas generator.

Table 1
Gaseous fuel properties [25,26].

Fuel properties	Hydrogen	Biogas	CNG
Density (kg/m ³)	0.07	1.2	0.7
Lower heating value (MJ/kg)	120	27.53	48–50
Flame Speed (m/s)	2.65–3.25	25	0.37–0.45
Self-ignition temperature (°C)	585	600–650	540
Flammability limits in air (% vol.)	4–70	7.5–14	5.3–14
Octane number	130	130	120

India provided Jatropha oil required for this research work. It is converted into Jatropha methyl ester (JME) using a two-step transesterification process and is then blended with diesel (purchased from a fuel station located in proximity to NIT Rourkela) in the proportion of 20% and 80% on a volumetric basis. Table 2 presents the properties of JME and JME20 along with diesel.

2.2. Engine modification

2.2.1. LHR engine

The LHR engine is formed by retrofitting a standard engine with thermal barrier coated (TBC) elements such as a piston, cylinder liner, cylinder block, cylinder head, and valves to reduce heat loss and increase work output. TBC on the engine components provides thermal insulation, causing the in-cylinder operation temperature to rise. The higher the operating temperature in the cylinder, the better the combustion and conversion of heat energy into useful work. Consequently, higher thermal efficiency, lower emissions, and lower brake-specific fuel consumption are achieved. For these reasons, there continues to be a significant amount of research and development (R&D) activities focusing on the development of TBC materials [27]. [Fig. 2 (a-b)] at the CSIR-Institute of Minerals and Materials Technology, Bhubaneswar, Odisha, India. TBC piston [Fig. 2 (c-d)] is replaced with the conventional piston in the CI engine to form the LHR engine before experimentation.

Yttria-stabilized zirconia and Cerium oxide (YSZ + CeO₂) are the TBC materials selected for the coating of the piston because their lower thermal conductivity and higher thermal expansion coefficient help in improving the thermal cycling life of the coated surface [28]. The addition of CeO₂ to YSZ improves the resistance to thermal shock because of high thermal expansion, the oxidation of the bond coat causes bare minimum stress, and mainly the monoclinic and tetragonal phases undergo a very slight phase transition. TBC materials are deposited on the piston by using atmospheric plasma spray (APS) coating process.

2.3. Test setup

The experimental study is carried out on a Kirloskar make, TAF1 model, 4-stroke, single-cylinder, air-cooled, direct injection (DI), naturally aspirated, diesel engine installed in the Heat Power Laboratory of the National Institute of Technology, Rourkela. Single-cylinder

Table 2
Test fuel properties.

Fuel properties	Test method	JME100	JME20	D100
Density (kg/m ³)	D 4052	880	857	850
Cetane number	D 976	48.13	47.35	47.14
Lower heating value (MJ/kg)	D 4806	38.45	42.85	43.5
Kinematic viscosity (m ² /s)	D 445	4.4 × 10 ⁻⁶	3.81 × 10 ⁻⁶	3.4 × 10 ⁻⁶
Flash point (°C)	D 93	170	77.2	50
Acid no. (mg KOH/g)	D 664	0.09	0.178	0.2
Surface tension (×10 ⁻³ N/m)		29.42	27.13	26.51
API gravity	D 287	29.11	35.47	38.77

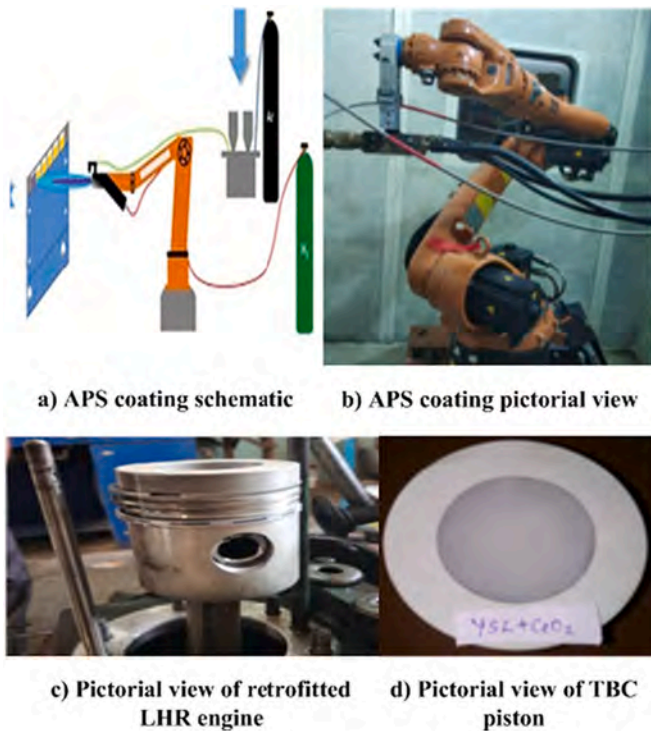


Fig. 2. (a-d) APS YSZ + CeO₂ coated piston retrofitted to the CI engine.

compression ignition (CI) engines are used in light weight transportation, small power generation, underground mining, defence, marine, load haul dumpers, stone crushers, sugar crane crushers, thrashers, concrete mixers, sprayer pumps, and agricultural applications in India. Greaves Cotton recently launched the world's cleanest single-cylinder Bharat Stage (BS) VI diesel engine for three-wheelers in 2019 [29]. The wide application is due to their high fuel efficiency, size flexibility, and durability. Single-cylinder engines are often more simple and compact. Table 3 presents the detailed single-cylinder engine specifications while Table 4 presents the nozzle specifications. At the beginning of the experimentation, the engine is run on neat diesel fuel at standard operating conditions. Further, the engine is modified to run in DFM. Fig. 3 represents the schematic of the experimental setup including all instrumental accessories. Load on the engine is applied using an eddy current dynamometer coupled to the engine shaft.

The rate of air consumption by the engine is measured by the pressure drop across an orifice with a discharge coefficient of 0.64. The pressure drop is calculated by measuring the height difference of the water column in a U-tube manometer which is fitted beside the air box. JME20 fuel consumption is determined by a burette to which a pair of optical fuel level sensors are attached at the top and bottom. HHO gas is produced by a wet cell electrolyzer at a flow rate of 0.75 LPM. The generated HHO gas is introduced along with air into the suction line through an extra pipe connection provided at the intake pipe. A flame arrester is installed between the wet cell electrolyzer setup, and the extra

Table 3
Engine specification.

Engine aspects	Specifications
Model	Kirloskar TAF1
Rated output (kW)	4.4
Rated speed (rpm)	1500
Bore (mm) × stroke (mm)	87.5 × 110
Compression ratio	17.5
Cooling type	Air cooling
Combustion chamber shape	Hemispherical
Piston type	Bowl-in-piston

Table 4
Nozzle specification.

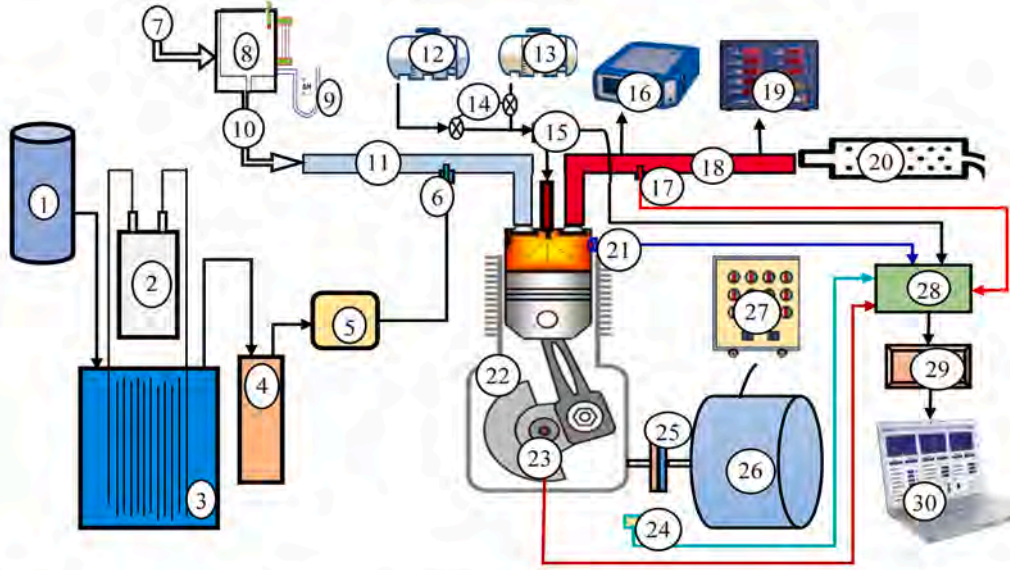
Nozzle parameters	Specification
Number of holes	3
Nozzle hole diameter (mm)	0.126
Angle between the holes (°)	120

pipe connected to the intake manifold to prevent the backfiring of HHO gas in the pipelines.

A K-type thermocouple is placed in the passage of the exhaust manifold and it measures the EGT. A Kistler-make 5395A model piezoelectric pressure transducer is placed on the engine cylinder head to record the in-cylinder pressure at every 0.6° CA. The pressure transducer transmits the signal to the data acquisition system (DAS) through a charge amplifier. In conjunction with the crank angle encoder, the cylinder pressure history concerning piston position is stored in a laptop using Legion Brothers software. A non-contact type speed sensor is positioned by the side of the flywheel and is used to measure engine speed. Heat release rate, ignition delay, and mass of fuel burned inside the cylinder are some of the important combustion characteristics which are determined by a combustion analyzer kit. The cyclic variation effect of the cylinder pressure is minimized by taking the mean data of 200 consecutive engine cycles which is used for analyzing combustion parameters like heat release rate, combustion duration, etc. The concentration of the regulated exhaust emissions (CO, HC, and NO) is measured by an exhaust gas analyzer (AVL 444) following ASTM D6522 standard procedure. Before conducting experiments, the moisture content of the exhaust gas is removed by using a condensation trap. Further, the exhaust gas is passed through a Non-Dispersive Infrared (NDIR) sensor which measures the concentration of CO, HC and CO₂. NO emissions are determined using an electrochemical device. HC and NO are measured in terms of parts per million (ppm) while CO and CO₂ are in percentage of volume (%Vol). AVL 437C smoke metre is used to measure smoke opacity. The raw emission data is converted to mass emissions (g/kWh) as per the Society of Automotive Engineers (SAE) standard [30].

2.4. Experimentation

Compression ratio (CR), fuel injection pressure (FIP), and the start of injection (SOI)/injection timing are some of the essential input parameters that influence the behavior of an engine run on an alternative fuel. Changing these variables may affect the engine performance. Optimization of these parameters is required to obtain the best results [31]. Initially, the conventional uncoated engine is run on neat diesel (D100) at the engine's original settings set by the manufacturer (17.5 CR, 200 bar FIP and 23 °CA bTDC SOI) at full load. The obtained experimental data is recorded to set the baseline data for comparison with the results that will be obtained for the HHO + JME20 dual-fuel operation on the LHR engine. After obtaining the baseline data, the engine is modified to LHR DFM. HHO gas is inducted along with air, while JME20 (pilot fuel) is injected into the cylinder via the fuel injector. The LHR engine is run on HHO + JME20 in DFM sequentially to conduct a set of pilot experiments, which are useful to decide the design of experiments. So, the set of pilot experiments is carried out by varying CR (16.5 to 18.5), FIP (200 to 280 bar), and SOI (21.5 °CA to 27.5 °CA bTDC). After performing the experiments, it is found that increasing the FIP beyond 260 bar and advancing SOI beyond 27.5 °CA bTDC results in rough engine operations. Hence, the maximum limit of the FIP and SOI is set to 260 bar and 27.5 °CA bTDC respectively. CR below 16.5 results in poor performance and CR above 18.5 cannot be achieved due to the manufacturing constraint. Table 5 presents the test matrix of the design of experiments. Taguchi approach is a statistical method generally used in the design and analysis of the experiments conducted. The design of experiments by Taguchi approach (L27 orthogonal) (3³) using Minitab software is selected in this study. A total of 27 experiments are performed to achieve



1. Electrolyte supply tank	2. DC Battery	3. HHO Gas generator	4. HHO Gas bubbler
5. Electrolyte separator	6. Flash back arrestor	7. Atmospheric air	8. Airbox
9. U-tube manometer	10. Filtered air	11. Suction line	12. Diesel tank
13. Alternative fuel tank	14. Valves	15. Fuel flow rate sensor	16. Exhaust gas analyzer
17. EGT Thermocouple	18. Exhaust line	19. Smoke meter	20. Silencer
21. Pressure transducer	22. CI Engine	23. Crank angle encoder	24. Speed sensor
25. Coupling	26. Dynamometer	27. Load cell	28. Control panel
29. Data acquisition system	30. Laptop		

Fig. 3. Engine experimental setup along with HHO gas generation system.

Table 5
Design of experiments.

Parameter	Level 1	Level 2	Level 3
CR	16.5	17.5	18.5
FIP (bar)	220	240	260
SOI (° CA bTDC)	24.5	26	27.5

all the possible combinations of the varying parameters which are given in Table 5. The engine operating conditions (CR, FIP, and SOI) and modification devices along with the methodology are given in Table 6.

2.5. Uncertainty analysis

The reliability of the experimental results can be determined by uncertainty analysis and hence calculation of uncertainty becomes significant to determine the fitness of the estimated parameters. To validate the precision of the experimental investigation, uncertainty analysis is done by performing three sets of experiments for every test fuel operation. Table 7 provides the accuracy, range, and uncertainties of instruments utilized in the present research work.

Uncertainty of the independent variable is evaluated by the Gaussian distribution approach [32], as given in Eq. (1), while uncertainty in the dependent variable is calculated using the root mean square approach given by Holman [33] which is mentioned in Eq. (2)

$$\Delta X_i = \pm \frac{2\sigma}{X_m} \quad (1)$$

Table 6
Methodology and devices in this study.

Variation of operating condition	Device/ methodology used
FIP (220, 240, and 260 bar)	As per the requirement, FIP is modified by using pressure tester
SOI (24.5, 26, 27.5 °CA bTDC)	0.3 mm thickness of shim is removed to advance 1.5° CA from standard injection timing 23° CA bTDC (So for 24.5 °CA one shim, 26 °CA two shims and 27.5 °CA three shims needs to be removed)
CR (16.5, 17.5, 18.5)	As per the requirement, CR is changed by keeping the respective thickness of gasket in between cylinder and cylinder head. Model calculation for single CR Compression ratio ₁ = CR ₁ = 1 + $\frac{V_s}{V_{c_1}}$ V_s = swept volume = $\frac{\pi}{4}D^2 \times L$ Clearance volume ₁ = V _{c₁} = V _{MG₁} + V _{CG} V _{CG} = Clearance volume without gasket = $\frac{\pi}{4}D^2 \times h_{CG}$ h _{CG} = Clearance height without gasket V _{MG₁} = Metal gasket volume = $\frac{\pi}{4}D^2 \times t_{MG_1}$ t _{MG₁} = Thickness of the metal gasket ₁ D = Bore diameter of cylinder L = Stroke length

$$\sigma = \sqrt{\frac{\sum_{i=1}^n (X_i - X_m)^2}{n-1}}$$

σ is the standard deviation while X_m is the mean of $n = 3$ sets of measured independent variable X_i

Table 7
Instrument uncertainties along with their ranges and accuracies.

Purpose of work	Used device	Accuracy	Range	Uncertainty (%)
Load on engine (Watt)	Resistive Load cell	±10	250–6000	±0.2
EGT (°C)	k-type thermocouple	±1	0–900	±0.5
Engine speed (rpm)	Non-contact type speed sensor	±10	0–10,000	±1
Cylinder pressure (bar)	Piezoelectric pressure transducer	±0.1	0–110	±0.15
Crank angle with respect to TDC (°CA)	Crank angle encoder	±0.6	0–720	±0.01
Fuel consumption (cm ³)	Burette	±0.2	1–30	±0.5
Digital conversion from analog (bit)	Data acquisition system	±0.1	64	±0.001
Gas flow rate (LPM)	Gas flow meter	±0.01	0–2.5	±0.02
NO (ppm)	Exhaust gas analyzer	± 50	0–5000	±1
HC (ppm)	Exhaust gas analyzer	±10	0–20,000	±0.5
CO (%)	Exhaust gas analyzer	±0.6	0–10	±0.03
Smoke opacity (%)	Smoke meter	±1	0–100	±1

$$\Delta R = \left\{ \sum_{i=1}^n \left(\frac{\partial R}{\partial X_i} \Delta X_i \right) \right\}^{0.5} \quad (2)$$

R is a function of the independent variable X_i , and n is the number of such, where ΔX_i denotes independent variables uncertainty, ΔR denotes dependent variable uncertainty.

The overall uncertainty of an experiment can be computed by using Eq. (3).

$$\text{Overall experiment uncertainty} = \sqrt{[\text{U of } \{(\text{BTE})^2 + (\text{BSEC})^2 + (\text{EGT})^2 + (\text{CO})^2 + (\text{HC})^2 + (\text{NO}_x)^2 + (\text{Smoke})^2\}]} \quad (3)$$

$$= \sqrt{[\text{U of } \{(0.5)^2 + (0.5)^2 + (0.5)^2 + (0.03)^2 + (0.5)^2 + (1)^2 + (1)^2\}]}$$

$$= 1.7323\%$$

The overall experiment uncertainty is = ± 1.7323 %.

3. Results and discussion

The combined effect of varying CR and fuel injection parameters (FIP and SOI) as per the design of experiments on the behavior of the LHR engine run on HHO + JME20 in DFM is investigated and discussed in this section. The obtained experimental results are plotted at full load condition for all the sets of experiments. For the sake of comparison, the baseline data of the diesel operation at full load, and the engine's original settings (17.5 CR, 200 bar FIP, 23 °CA bTDC SOI) are represented in dashed lines for all the combustion, performance, and emission results. This study also looks at how pilot fuel spray characteristics affect engine performance and emissions as nozzle injection pressure changes.

3.1. Effect of spray

Several researchers [34–36] reported that fuel injection pressure (FIP) affects spray characteristics of the test fuel. The spray characteristics of the fuel entering the combustion chamber influence air-fuel mixing and subsequently affect engine performance and emissions. The major spray characteristics are spray penetration length, spray break-up length, spray cone angle, and sauter mean diameter (SMD). To characterize the spray, expressions for droplet size distribution and mean diameter are desirable. An appropriate and commonly used mean diameter is SMD. The FIP of the test fuel has a large influence on the spray characteristics, which in turn affect the performance and emission characteristics of the engine. So, SMD is one of the spray parameters used to evaluate the influence of FIP. SMD is also one of the main inputs used to calculate a few other spray characteristics [37].

SMD is the average diameter of the test fuel droplet that has a same volume to surface area ratio as that of the total spray. The SMD of the test fuel represents the atomization characteristics of the injected spray, which plays an important role in improving or degrading engine performance and emission parameters. The Hiroyasu model [38] was used to calculate the SMD (X_{32}) for complete sprays after incorporating the ambient pressure effect as given in Eq. (4).

$$\frac{X_{32}}{D} = 0.38Re^{0.25}We^{-0.32} \left(\frac{\mu_l}{\mu_g} \right)^{0.37} \left(\frac{\rho_l}{\rho_g} \right)^{-0.47} \quad (4)$$

where “ X_{32} ” represents sauter mean diameter, “ Re ” indicates Reynolds number = $\frac{V_l D}{\nu_l}$, “ We ” is the Weber's number = $\frac{V_l^2 D \rho_l}{\sigma_l}$, “ V_l ” is velocity of test fuel = $c_d \sqrt{\frac{2\Delta p}{\rho_l}}$, and “ D ” is nozzle diameter. “ ρ_l , ν_l , μ_l and σ_l ” are density, kinematic viscosity, dynamic viscosity and surface tension of liquid test fuel respectively. The Weber number is key parameter for SMD and it is function of density and surface tension. As the surface tension is higher with JME20. Weber number would be lower. Hence, lower Weber number would give larger SMD with biodiesel-diesel blend [37]. The obtained SMD values with respect to FIP for the test fuels are plotted in Fig. 4.

It can be observed from the figure that the SMD values decrease at higher injection pressure. When the SMDs of the two fuels are compared at all injection pressures, the SMD of JME20 is found to be greater than that of D100 because JME20 has slightly higher fuel viscosity, density, volatility and flow point than D100. The larger droplets produced by JME20 spray will lead to poor atomization and less air entrainment. Less air entrainment will limit the vaporization of JME20 [37]. Bigger SMD values represent larger fuel droplet sizes, which imply a smaller number of droplets. As the number of droplets is smaller, the surface area of the droplets in contact with the gaseous fuel reduces, which reduces the evaporation of the liquid droplets, thereby resulting in inferior atomization when compared to D100 [39]. However, when JME20 is used in dual-fuel mode along with HHO, the mixing effect is enhanced due to the high diffusivity of the gaseous fuel. Also, the presence of oxygen in both JME20 and HHO contribute to better combustion. At higher FIP, there is a fast breakup of the fuel droplets along the length of the spray, which decreases the SMD. The reduction in SMD enhances the entrainment of air into the spray. The increase in the quantity of air entrained has a greater tendency to promote vaporization of the spray [39].

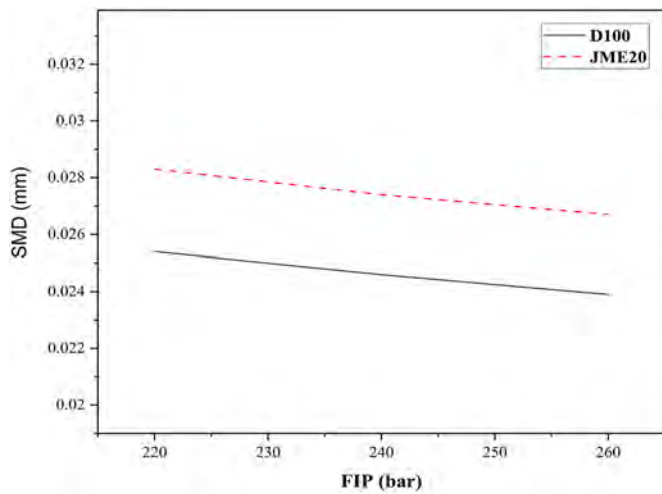


Fig. 4. Test fuel sauter mean diameter (SMD) with injection pressure.

3.2. Combustion analysis

3.2.1. Cylinder pressure history

In-cylinder pressure, HRR, and ignition delay are significant parameters affecting the combustion process. The cylinder pressure history is very important to understand the combustion, performance, and emission characteristics of the engine [30]. The pressure-crank angle curve for D100 at the engine's original settings on the standard engine, and HHO + JME20 at different engine operating conditions on the LHR engine is shown in Fig. 5 (a-i) at full load. The peak in-cylinder pressure (P_{max}) for neat diesel (D100) is about 63.13 bar at 376.8°CA (full load), P_{max} in DFM is higher than D100 at every test condition and shifts towards the top dead centre (TDC). The ceramic-coated piston in the LHR engine retains the high-temperature combustion environment which leads to the complete combustion of fuel, resulting in higher P_{max} . The prominent combustion characteristics of HHO also result in higher combustion temperature leading to higher P_{max} . Similar findings were

reported by Rimkus et al. [40] in their experimental investigation of a CI engine operated on HHO gas.

Irrespective of any given fuel injection parameters, on increasing CR from 16.5 to 18.5, the P_{max} value increases. Due to the reduced clearance volume at a higher CR, the in-cylinder temperature and pressure increase after compression. This reduces ignition delay and enhances the combustion process resulting in a higher combustion temperature. Chintala and Subramanian [41] reported similar observations in their research work related to dual-fuel operation with hydrogen-diesel. Early injection fuel leads to more fuel accumulation, which forms a rich mixture inside the cylinder and supports higher premixed combustion in the initial stages. This increases the in-cylinder pressure and shifts P_{max} towards TDC. When fuel is injected at 26 °CA bTDC the peak cylinder pressure is observed to be maximum at the given CR and fuel injection pressure (FIP). For instance, at 18.5 CR and 240 bar, advancing SOI from 24.5° to 26°CA bTDC, increases P_{max} from 68.9 bar to 70.9 bar and shifts it from 369.4°CA to 368.3°CA.

Advancing SOI to 27.5°CA bTDC results in poor mixing of fuel and air, and hence there is a lower in-cylinder pressure. As the FIP is increased from 220 to 240 bar, P_{max} increases at all engine conditions. One of the reasons could be enhanced combustion due to proper atomization and uniform air-fuel mixing [31]. The maximum P_{max} is observed at 18.5 CR, 240 bar, and 26°CA bTDC, which is higher than diesel by about 70.9 bar (12.3%). This is due to the combined effect of enhanced combustion temperature, proper air-fuel mixing, and finer atomization of the fuel.

3.2.2. Ignition delay

Ignition delay (ID) is the elapsed time from the start of injection (SOI), and the start of combustion (SOC). The delay depends on the CR, atomization of fuel droplets, fuel injection timing, engine speed, and intake air temperature [42]. The pattern of the ignition delay for the HHO + JME20 operation in the LHR engine at varied CR, FIP, and SOI is presented in Fig. 6 (a-c). The delay found for D100 at full load is 12.4°CA which is represented by a dashed line. In a dual-fuel LHR engine, the type of fuel plays a vital role in deciding the ignition delay [40]. The higher Cetane value of JME20 [30] along with higher diffusive nature of

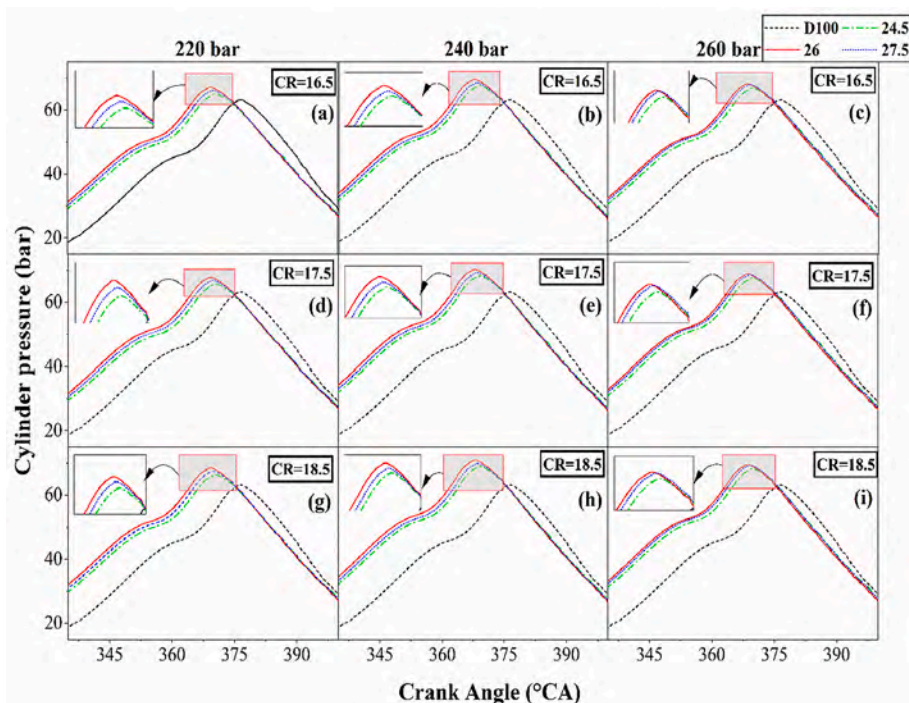


Fig. 5. (a-i) Cylinder pressure history.

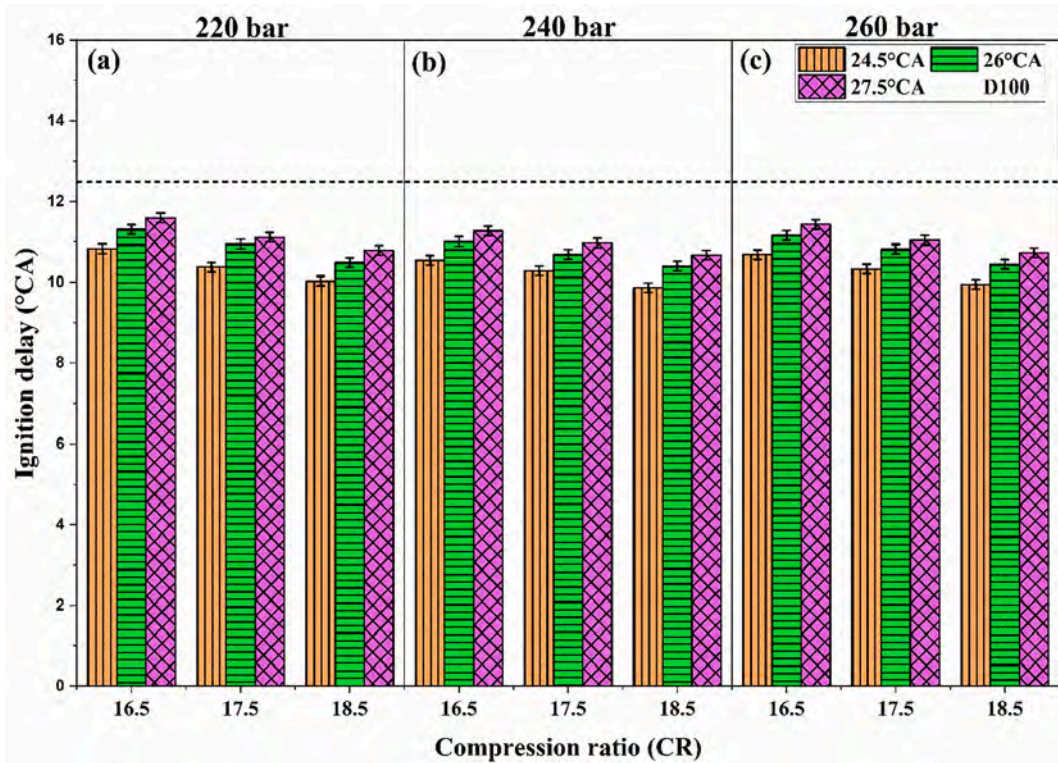


Fig. 6. (a-c) Ignition delay with respect to variation of CR and fuel injection parameters.

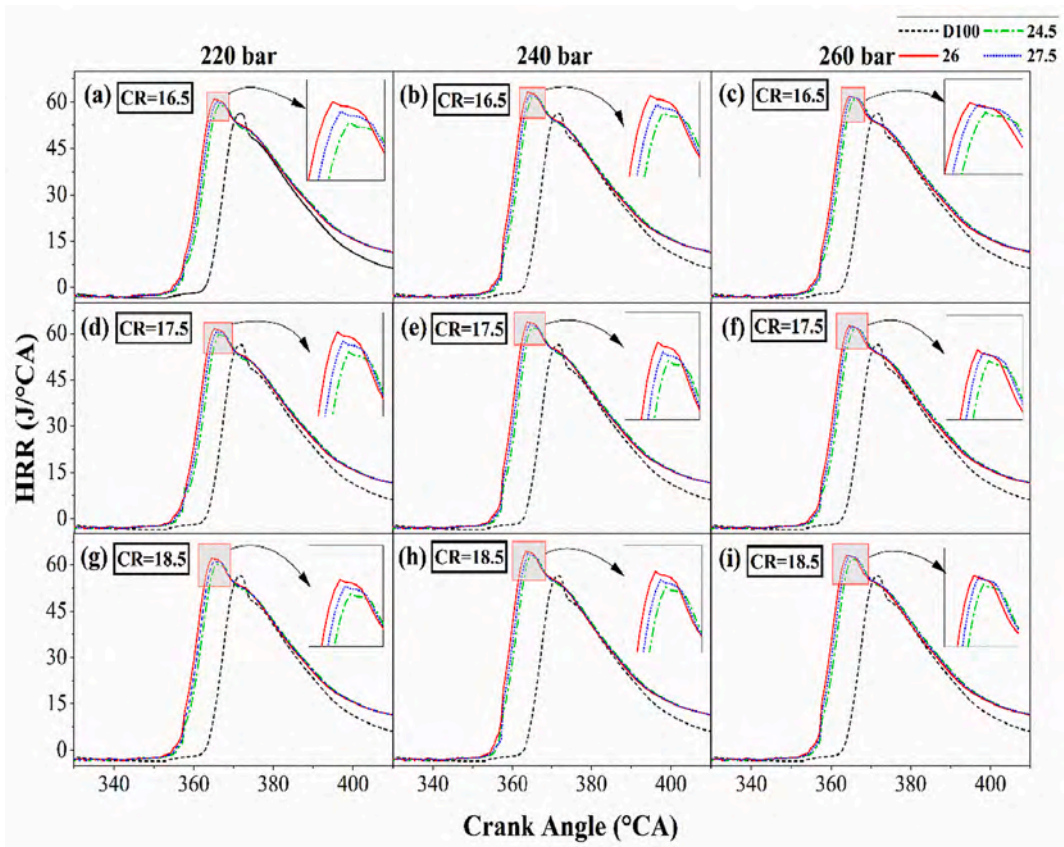


Fig. 7. (a-i) Variation of HRR with respect to crank angle at different test conditions.

HHO results in shorter ignition delay than the baseline fuel at all the engine test conditions [19]. A shorter ignition delay is preferred in a CI engine to achieve smoother combustion resulting in better performance of the engine [6]. The temperature and pressure of the charge after the compression process play a vital role in affecting the ignition delay. So the rise of in-cylinder temperature (also due to the TBC piston insulation) leads to early ignition of the fuel, and hence there is a reduction of the ignition delay [27].

A declining trend of the ignition delay is observed for a higher compression ratio at the given fuel injection conditions. This is due to the increase in the in-cylinder pressure and temperature after compression at higher CR leading to shorter delay and smaller combustion duration. The findings are in agreement with an earlier research work [43]. As the SOI is advanced from 24.5 to 27.5 °CA bTDC, the delay increases marginally. As observed in a previous study [44] this might be due to the lower in-cylinder pressure and temperature at the time of fuel injection. It is also noticed from Fig. 6 (a-c) that increasing FIP from 220 to 240 bar at a given CR, and SOI timing shortens the delay as well as the combustion duration. This may be due to the reduction in the droplet size of the pilot fuel resulting in finer atomization and faster evaporation [45]. However, the ignition delay increases moderately at 260 bar in comparison with 240 bar. For instance, at 27.5 °CA bTDC SOI and 16.5 CR, on increasing the FIP from 240 to 260 bar an extended delay is noticed. This deviation in the pattern may be attributed to the reduced momentum of the fuel droplets [45]. The delay is found to be about 10.4 °CA at CR 18.5, 240 bar, 26 °CA bTDC which is lower than D100 at full load by about 2 °CA.

3.2.3. Heat release rate

Heat release rate (HRR) also referred to as apparent net heat release rate is obtained by the correlation given in Eq. (5) [46].

$$\frac{dQ_n}{dt} = \frac{\gamma}{\gamma - 1} P \frac{dV}{dt} + \frac{1}{\gamma - 1} V \frac{dP}{dt} \quad (5)$$

Here Q_n is the apparent net heat release rate, γ is the specific heat ratio, P and V are instantaneous in-cylinder pressure and volume

respectively. For measuring HRR, the mean of 200 consecutive engine cycles cylinder pressure data is taken for minimizing cyclic variation effect. At full load, the HRR curve for D100 on standard engine operation and HHO + JME20 operation in the LHR engine by varying engine operating conditions is shown in Fig. 7 (a-i). The maximum heat release rate (HRR_{max}) for D100 is around 56.4 J/°CA at 371.5 °CA at full load. The HRR is maximum during the uncontrolled combustion phase. The higher heating value of HHO with its higher flame speed and the heat trapped from the previous cycle by the TBC piston [47] accelerate the uncontrolled combustion phase leading to higher HRR in the LHR engine run in DFM [19].

Irrespective of the fuel injection condition, as the CR is increased from 16.5 to 18.5, the HRR increases. The in-cylinder pressure and temperature increase as a result of the decrease in the clearance volume at higher CR. This causes enhanced combustion resulting in higher HRR. Advancing SOI from 24.5 to 26 °CA bTDC increases ignition delay resulting in higher HRR [31]. Higher FIP causes finer atomization of the pilot fuel leading to better air-fuel mixing and more fuel accumulation shortening the combustion duration. A similar finding is recorded in this work when the FIP is increased from 220 to 240 bar. Increasing FIP to 260 bar and beyond decreases the HRR values due to inferior atomization and fuel impingement on cylinder walls causing incomplete combustion [45]. The combined effect of advancing SOI and increasing FIP along with higher CR results in higher HRR. The highest HRR_{max} among the engine test conditions is observed to be 64.5 J/°CA at CR 18.5, 240 bar, and 26 °CA bTDC at full load. The combined effect of finer atomization and better mixing of the pilot fuel with the gaseous fuel is the reason for this result.

3.3. Performance

3.3.1. Brake thermal efficiency (BTE)

BTE is highly influenced by air-fuel mixture, the calorific value of fuel, CR, engine load, and SOI [42]. Fig. 8 (a-c) show the variation of BTE with respect to varying CR, FIP, and SOI for HHO + JME20 operation in the LHR engine at full load. The BTE value for D100 is about

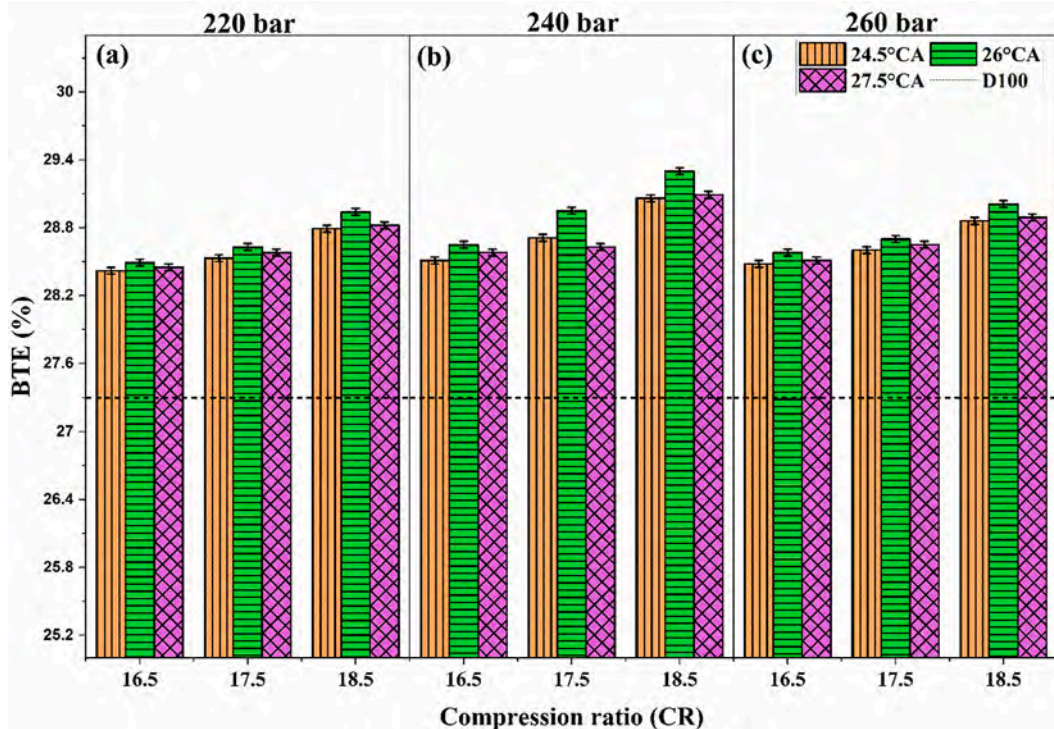


Fig. 8. (a-c) BTE with respect to varying CR and fuel injection parameters.

27.3% (presented as a dashed line) at full load. The BTE for the dual-fuel operation is higher than the D100 operation at all varying engine conditions. The enhanced BTE is due to the combined effect of high in-cylinder temperature caused by the TBC piston and high calorific hydrogen (which is present in HHO) combustion [11]. As previously stated, CR is one of the major parameters influencing BTE; experiments reveal that increasing CR promotes BTE at given fuel injection parameters [48]. For a given CR and FIP, advancing SOI from 23 °CA bTDC to 26 °CA bTDC further improves BTE. This is because as the SOI advances, the pressure and temperature inside the cylinder are lower, which prolongs the delay, thereby providing sufficient time for adequate mixing of primary and pilot fuels with air [6,31]. It can be observed that advancing beyond 26 °CA bTDC decreases the peak cylinder pressure, results in shifting the peak cylinder pressure from the TDC, and decreases power output. This decreases the BTE under all other varying conditions, deviating from the optimum value of the SOI from given conditions [42].

Increasing FIP from 220 bar to 240 bar enhances the BTE, which is due to reduction in SMD of JME20 which is already witnessed in the earlier findings as shown in Fig. 4. The decreased SMD of JME20 droplets helps in increases of droplet surface area which facilitates more heat transfer between compressed air and fuel droplet results in better vaporization [39,49]. However, a reduction of BTE is observed at 260 bar when compared to the corresponding BTE values at 220 and 240 bar. This is because, at 260 bar, the droplets become finer and their momentum is insufficient to properly distribute the fuel in the cylinder, resulting in a poor air-fuel mixture and, ultimately, poor combustion [45]. The highest BTE of 29.1% is observed at CR 18.5, 240 bar, and 26 °CA bTDC which is 6.6% higher than baseline diesel data.

3.3.2. Brake specific energy consumption (BSEC)

BSEC is the amount of fuel energy required to generate 1 kW of brake power as the output. Mathematically, it is equal to the product of brake-specific fuel consumption (BSFC) and lower heating value (LHV) of the test fuel [42]. Fig. 9 (a-c) depicts the variation of BSEC with varying fuel injection parameters and CR of the LHR engine run in DFM with HHO +

JME20.

The BSEC value for D100 at normal operating conditions is found to be about 15.9 MJ/kg-kWh. BSEC for HHO + JME20 operation in the LHR engine is lesser than conventional diesel for all the test conditions. This may be attributed to the higher energy released by HHO gas. The low thermal conductivity of the YSZ + CeO₂-coated piston has the capability of inhibiting heat energy that can be converted into useful work. As a result, the BSEC is reduced in the LHR engine [47]. A decreasing trend of the BSEC is observed with increasing CR. This trend is valid for all given fuel injection parameters. This trend is due to a higher CR that increases the in-cylinder pressure and temperature improving BTE and fuel economy [48].

Advancing SOI to 26 °CA bTDC leads to the burning of a significant quantity of fuel in the premixed combustion phase resulting in rapid HRR and higher brake power thereby reducing the BSEC values compared to other SOI at given CR and FIP [44,50]. Advancing the SOI further leads to an improper air-fuel mixture that increases BSEC slightly. Kanth et al. reported a similar trend in their hydrogen-biodiesel dual-fuel experiment [31]. A combination of CR 18.5, 240 bar, and 26 °CA bTDC gives the least BSEC of 14.86 MJ/kWh. The optimized engine operating conditions for the BSEC are the same as that of the optimized engine operating conditions for BTE.

3.3.3. Exhaust gas temperature (EGT)

EGT is majorly influenced by the quality of fuel, engine load, CR, fuel injection pressure and SOI. Fig. 10 (a-c) represent the variation of EGT with respect to varying CR, FIP, and SOI of HHO + JME20 operation in the LHR engine. The EGT for D100 is recorded as 291 °C at full load. The EGT for the HHO + JME20 operation in the LHR engine is found to be higher than the baseline diesel operation irrespective of the engine operating conditions. This is due to the high in-cylinder temperature generated by the combined effect of enhanced combustion with HHO (due to high flame velocity and high diffusive nature of HHO gas) and accumulated heat energy by the TBC-coated piston. Also, JME20 tends to shift the combustion process towards the diffusion phase because of its higher viscosity and lack of volatility, contributing towards higher

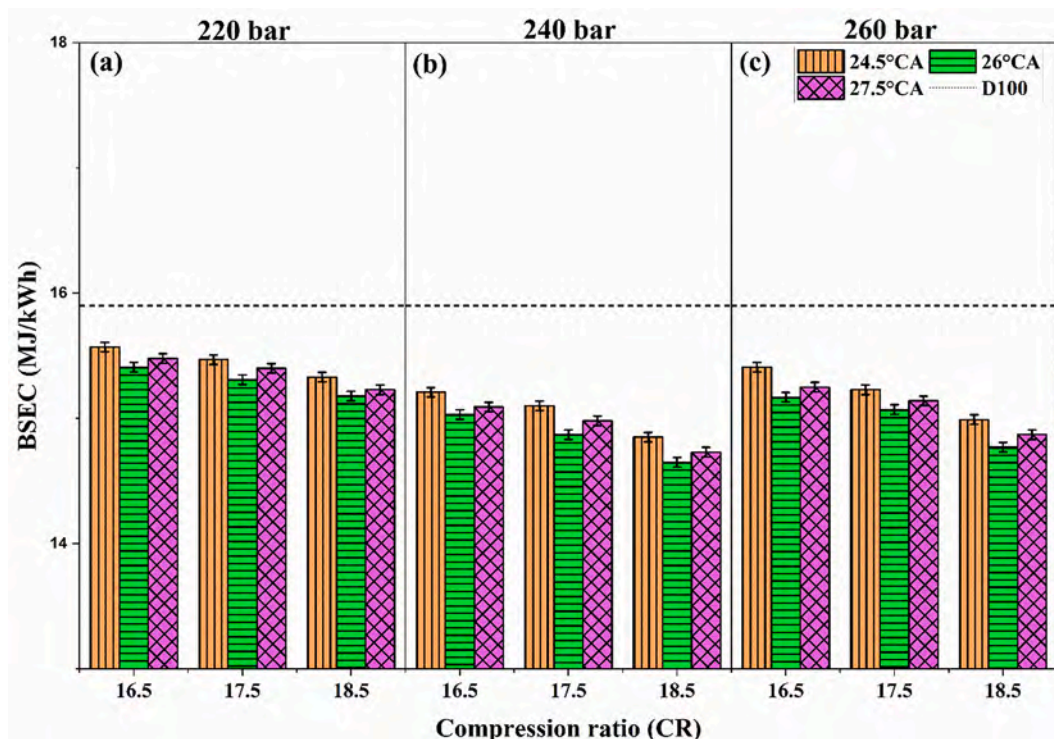


Fig. 9. (a-c) BSEC with respect to CR at varying fuel injection parameters.

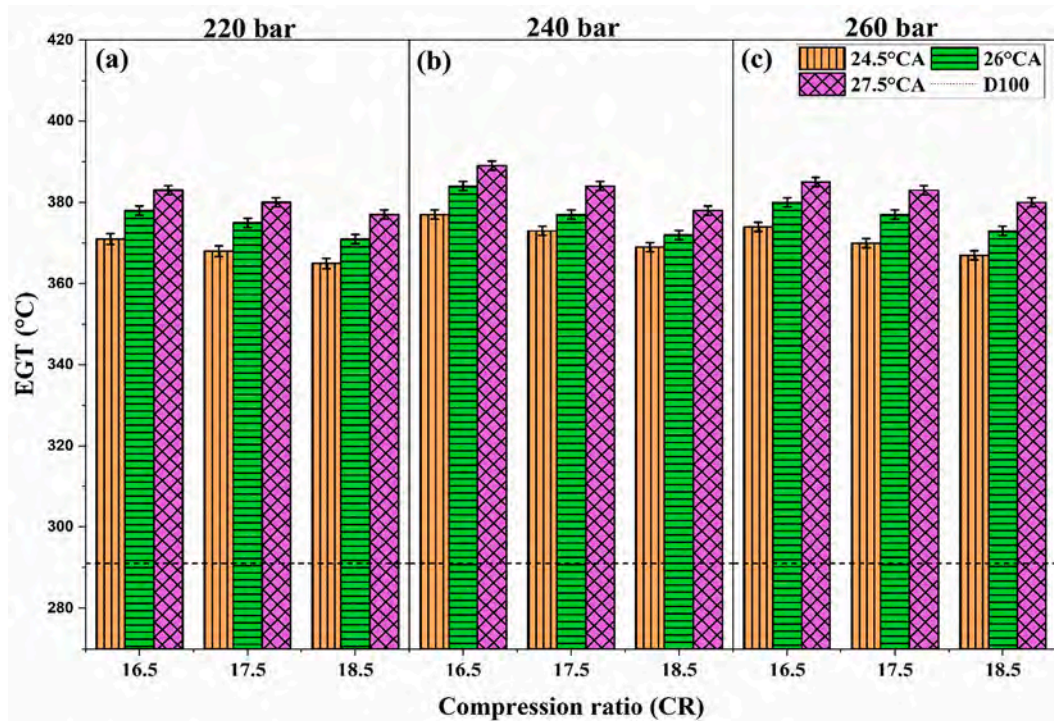


Fig. 10. (a-c) EGT with respect to varying CR and fuel injection parameters.

EGT [30]. It is observed that with the increment in the CR, the EGT reduces. This trend is noted for all varying fuel injection parameters at full load. This must be due to the reduced ignition delay at higher CR causing faster burning rates and shorter combustion duration resulting in lower EGTs [48].

Advancing the SOI results in more accumulation of fuel giving a fuel-rich mixture and thus there is a higher EGT. A similar finding is reported

by Gorle et al. [51] in their optimization work on a CI engine operating with Jatropha biodiesel. Also, advancing the SOI results in more burnt gases getting compressed when the piston moves towards the TDC which raises the temperature of exhaust gases. Higher values of EGT are observed at 240 bar than at 220 bar for given SOI and CR, As the fuel injection pressure is increased, the SMD of JME20 enhances the rate of combustion in the premixed combustion phase due to finer spray

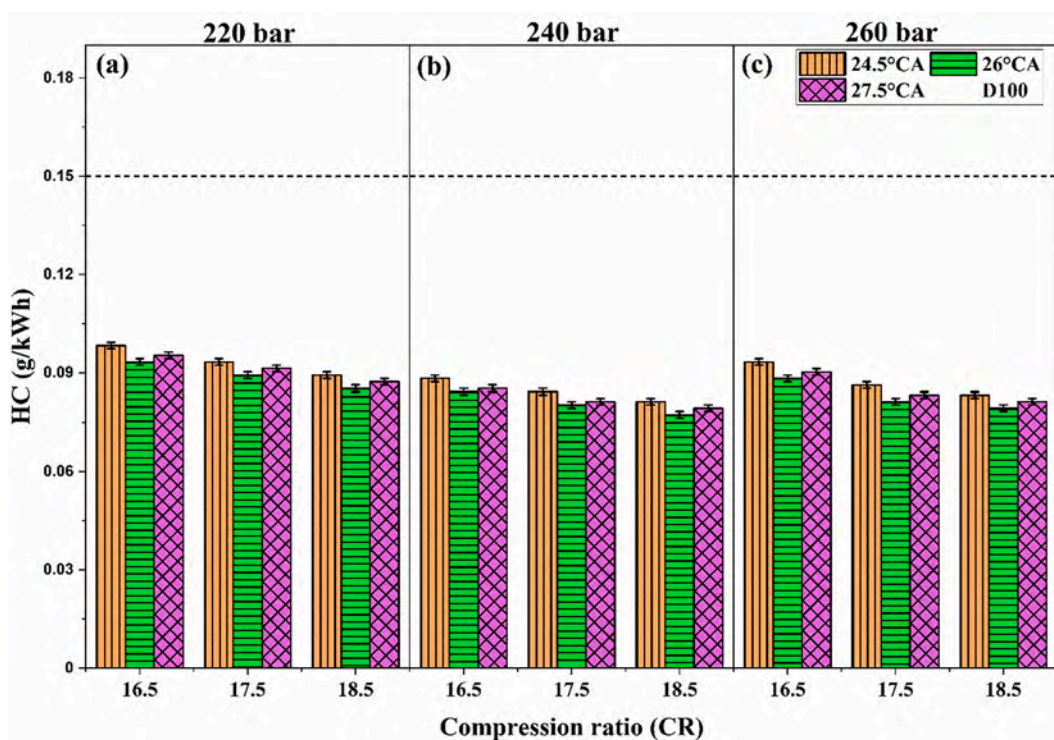


Fig. 11. (a-c) HC emission variation with CR at varying fuel injection parameters.

atomization resulting in an improved air-fuel mixture [52]. Increasing pressure to 260 bar results in a slight reduction of the EGT values because of too much reduction in the size of the fuel droplets leading to improper combustion [31].

3.4. Emissions

3.4.1. Unburnt hydrocarbon (HC)

Fig. 11 (a-c) represent HC emission found in the exhaust gas at varying engine operating conditions of the LHR engine in the HHO + JME20 operation. HC emission in the diesel operation is found to be 0.15 g/kWh. The combustion process is enhanced by the reduction of the quenching distance with the increased temperature of the TBC piston. Better combustion characteristics of HHO, keep HC emission at a bare minimum level compared to that of D100 at all test conditions. The increased temperature will also assist during the after-burning stage in the exhaust pipe [53]. Irrespective of fuel injection conditions, as the CR is increased, the in-cylinder temperature increases leading to a reduction in HC emissions. The rate of HC oxidation depends exponentially on in-cylinder temperature as given in the empirical correlation (6) which is mentioned by Heywood [42].

$$\frac{d[HC]}{dt} = -6.7 \times 10^{15} e^{\left(\frac{-18,735}{T}\right)} x_{HC} x_{O_2} \left(\frac{P}{RT}\right) \quad (6)$$

At given CR and FIP, advancing SOI from 24.5 to 26 °CA bTDC reduces HC emissions moderately. This is accredited to early injection which enhances air-fuel mixing because of the availability of time contributing towards better combustion. Nevertheless, advancing beyond 26 °CA bTDC increases the HC emissions. The prolonged delay must be the reason for the discrepancy in the trend. It creates more fuel-rich zones in the combustion chamber which are not completely oxidized leading to the formation of unburnt HC [31].

Larger droplets evaporate more slowly, increasing the likelihood of incomplete combustion. Although JME20 shows larger SMD fuel

droplets than D100, HC emissions are observed to be less when compared to D100 at each test condition. This may be due to the induction of HHO gas in dual-fuel mode. As the FIP is increased, the SMD of droplets decreases, which is a favourable condition contributing towards complete combustion [49]. However, increasing FIP beyond 240 bar results in a slight increase in HC emissions. The reason for such a diversion in the pattern must be due to fuel impingement on the cylinder wall and piston cavity, which could not burn. With increasing FIP up to 260 bar, the velocity with which the fuel is injected increases, and thus the impingement of the fuel on the cylinder walls dominates, preventing the fuel from participating in combustion and increasing HC emissions [52]. The least HC emission is found to be 0.079 g/kWh at 18.5 CR, 240 bar, and 26 °CA bTDC which is 47.3% lower than baseline diesel data at full load.

3.4.2. Carbon monoxide (CO)

Fig. 12 (a-c) display the trend of CO with the varying engine operating parameters for the HHO + JME20 operation in the LHR engine. CO emission for D100 operation is recorded to be 3.4 g/kWh at full load. The LHR engine with the HHO + JME20 operation shows lower CO emissions than the D100 operation which can be seen in Fig. 12 (a-c). This is because of the following local factors (i) oxygen content in both the fuels (HHO and JME20 [54]) helps oxidize CO to CO₂ (ii) better mixture ratio helps in better combustion (iii) pressure and (iv) temperature retained by the TBC piston supports better combustion [55,56].

At higher CR, CO emissions are reduced due to the increase in the in-cylinder pressure and temperature which result in rapid burning and complete combustion of fuel [48]. A consistent reduction in CO is observed when the pilot injection is advanced from 24.5 to 26 °CA bTDC at any set CR and FIP. This may be due to the longer time available for the fuel droplets to vaporize and mix with the gaseous fuel which enhances the combustion process [44]. Advancing to 27.5 °CA bTDC leads to more local fuel-rich regions which are not oxidized completely, and hence more CO emissions are noticed. In CI engines, CO emission is the result of improper oxidation reactions caused by the low availability of

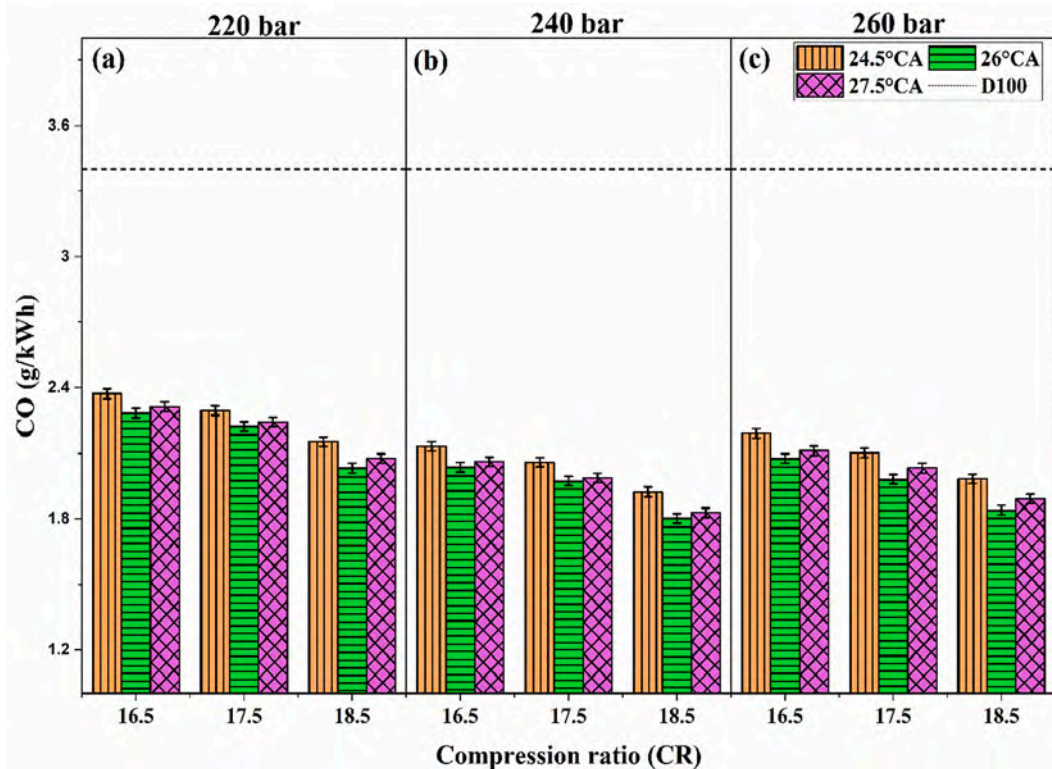


Fig. 12. (a-c) CO emission variation with CR at varying fuel injection parameters.

oxygen. When compared to D100, JME20 has higher SMD values and a longer spray penetration length. The higher SMD values cause slow evaporation of the fuel droplets, leading to inferior atomization [57]. This is reason for incomplete combustion. The larger spray penetration length of JME20 causes impingement of the fuel on the piston surface, due to which the impinged fuel does not take part in combustion chemical reactions. However, despite the inferior spray characteristics of JME20 compared to D100, the induction of HHO results in lesser CO emissions compared to D100. This is most likely due to the presence of oxygen in both HHO and JME20, which promotes oxidation, and thus converts the majority of CO to CO₂ [36,49]. However, 260 bar FIP shows higher CO emissions than 240 bar. This is probably due to the poor pre-mixed combustion phase which results in a lower in-cylinder temperature restricting the oxidation of CO. The lowest CO emission in DFM with HHO + JME20 operation is found to be about 1.902 g/kWh at 18.5 CR, 240 bar and 26 °CA bTDC which is 44.1% lesser than D100.

3.4.3. Smoke

Smoke opacity is an indirect measurement of PM, which gives continuous real-time results even in transient operation reported by Black et al. [58]. Further, the smoke opacity data shall help the reader to understand the basic idea of pollutant forming [59] in LHR dual-fuel engine. Fig. 13 (a-c) depict the variation of smoke opacity at varying test conditions of the LHR engine run on HHO + JME20. The conventional diesel operation shows smoke opacity of around 35.8% at full load. The smoke meter reveals lesser smoke opacity in the dual-fuel operation in the LHR engine than the conventional diesel operation for all the test conditions. The in-cylinder temperature retained by the TBC piston helps in reduction of physical and chemical delays which in turn reduces smoke opacity [47]. The higher in-cylinder temperature also assists in the oxidation of soot [53]. The presence of oxygen and the carbon-free nature of HHO are some of the reasons for reduced smoke opacity. With the increase in the CR from 16.5 to 18.5 it can be observed that smoke opacity shows a declining trend at any fuel injection parameter. This may be due to the higher in-cylinder temperature after compression which leads to better oxidation of the fuel. Earlier injection

of fuel from 24.5 to 26 °CA bTDC decreases smoke opacity due to an adequate amount of pilot fuel thoroughly mixed with the gaseous fuel ready for combustion providing a faster flame front covering the whole combustion zone [60]. Advancing injection timing further to 27.5 °CA bTDC causes poorer combustion due to inadequate equivalence ratio which increases smoke opacity. Large fuel droplets cause incomplete combustion, which is one of the reasons for smoke formation [39]. JME20 shows larger SMD values than D100 at each FIP. However, experimental results show that JME20 + HHO produces less smoke than D100. This may be due to the presence of chemically bounded oxygen in both fuels, which promoted soot oxidation.

The increase in FIP narrows the range of the droplet diameters, which means the droplet size distribution is forced towards a uniform distribution and the portions of the largest and smallest droplets are reduced there by proper air-fuel mixing, and finer droplet formation takes place at higher FIP, which contributes towards the complete combustion of the fuel [61]. However, at 260 bar a reverse trend is noticed due to poor combustion caused by lesser momentum of fuel droplets. The smoke opacity is recorded to be 26.9% when the engine is set to 18.5 CR, 240 bar, and 26 °CA bTDC.

3.4.4. Nitric oxide (NO)

The NO formation is majorly affected by in-cylinder temperature, availability of oxygen, and residence time [30,62]. Fig. 14 (a-c) depict NO variation with respect to CR at different fuel injection conditions of the LHR engine run on HHO + JME20 at full load. Some principal reactions for the NO formations from the nitrogen present in the air inducted are stated below in Eqns. (7–9) [42].



The NO value in exhaust emissions with D100 operation is noted to be 5.6 g/kWh at full load. The LHR engine run on DFM emits higher NO than the D100 operation at all test conditions. The availability of oxygen

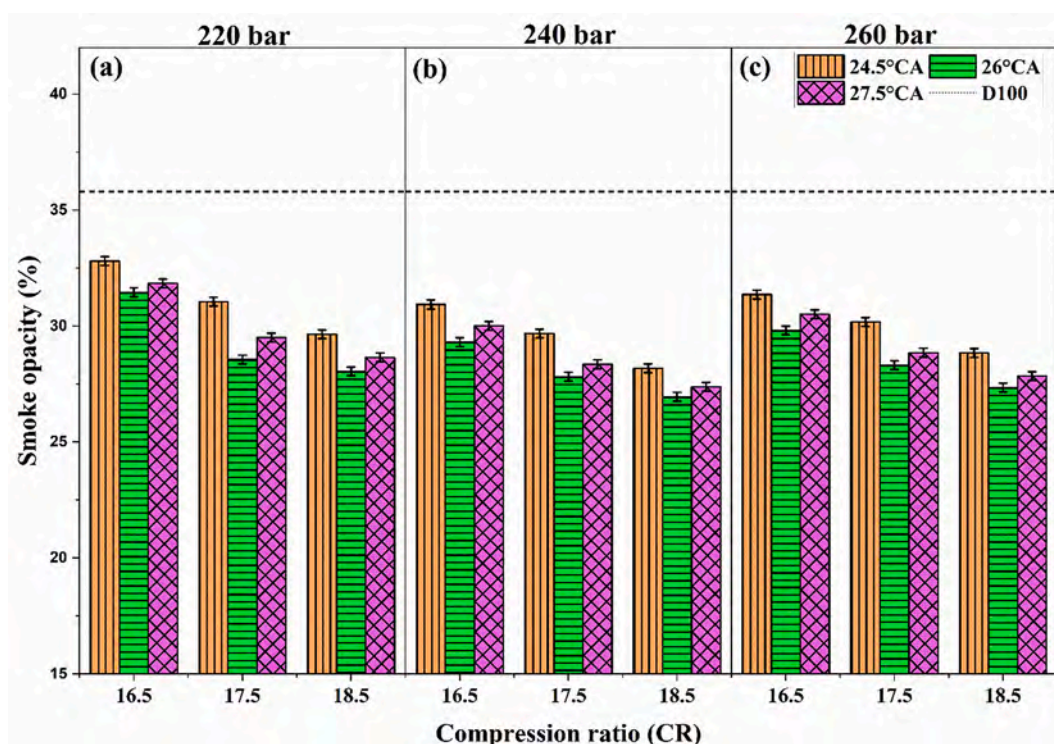


Fig. 13. (a-c) Smoke opacity variation with CR at varying fuel injection parameters.

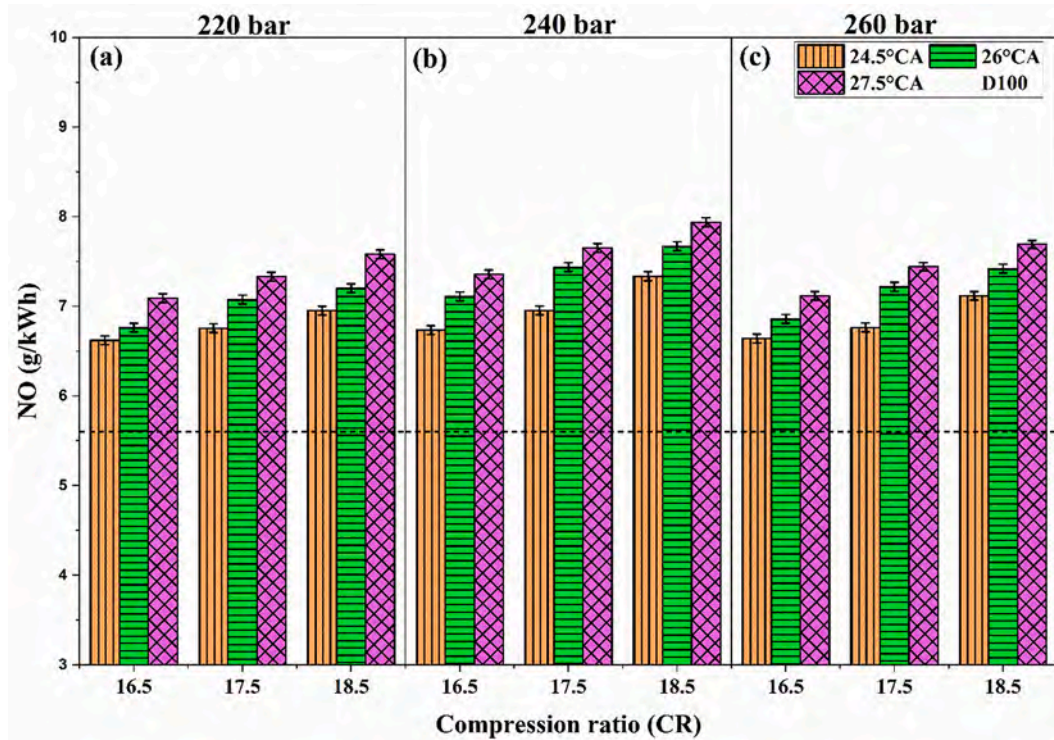


Fig. 14. (a-c) NO variation with CR at varying fuel injection parameters.

in HHO as well as Jatropha biodiesel must be one of the factors responsible for higher NO emissions. A similar justification was given by Gad et al. [63] in their work on HHO enrichment with biodiesel. Additionally, higher in-cylinder temperature formed in DFM due to combustion of hydrogen in HHO and temperature of combustion retained by the TBC piston by reducing heat loss may have contributed to higher NO emissions.

Increasing the CR increases the in-cylinder temperature which promotes NO formation [48]. This is why that NO emissions are higher for CR of 18.5 at any given fuel injection condition. For 16.5, 17.5, and 18.5 CR, NO emission is recorded as 6.94, 7.23, and 7.51 g/kWh, respectively, at 240 bar, and 26 °CA bTDC. According to the findings of this study, early fuel injection into the cylinder causes more NO emissions. It is understood that advancing fuel injection prolongs the ignition delay due to which more time is available for NO chemistry. Additionally,

advancing SOI leads to a higher heat release rate which may have contributed to the NO formation [44]. With the increase in FIP from 220 to 240 bar, the SMD values decrease which leads to enhanced atomization and mixing process of the pilot fuel with the gaseous fuel. A homogenous mixture results in higher HRR and maximum temperature which promotes formation of NO. However, DFM shows higher NO at all operating conditions compared to D100 single fuel mode operation. This may be due to oxygen present in JME20 and HHO which oxidize N₂ thereby promoting NO formation [49]. Except at 260 bar, NO emissions are slightly lower than that produced at 240 bar. This may be due to improper air-fuel mixing which lowers the in-cylinder temperature thereby consequently lowering NO emissions than those produced at 240 bar. A comparative analysis (in terms of percentage) of the LHR engine run on HHO + JME20 at the identified optimized conditions (18.5 CR, 240 bar, and 26 °CA bTDC) with the standard diesel engine operation as a reference line at full load is shown in Fig. 15.

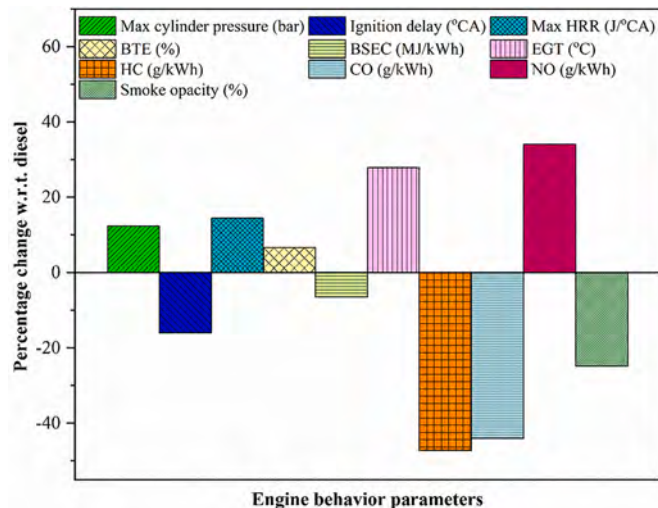


Fig. 15. Comparative analysis of LHR engine with base line diesel data.

4. Conclusions

The following are the key findings drawn from the experimental results obtained from running a single-cylinder, LHR dual-fueled CI engine on HHO + JME20 at different engine operating conditions (varying CR, FIP, and SOI).

- The peak cylinder pressure for dual-fuel operation increases with the increase of CR from 16.5 to 18.5. The maximum peak cylinder pressure among all test conditions is recorded to be 70.9 bar at 18.5 CR, 240 bar FIP, and 26 °CA bTDC SOI.
- There is an increase in maximum HRR with the increase in CR from 16.5 to 18.5. At 18.5 CR, 240 bar FIP, and 26 °CA bTDC SOI, the maximum HRR is found to be 64.5 J/°CA which is relatively higher by 14.3% than D100 at full load.
- The highest BTE of 29.1% is observed for DFM at 18.5 CR, 240 bar FIP, and 26 °CA bTDC SOI which is higher than the BTE of conventional diesel operation at full load by 6.6%.

- At 18.5 CR and 240 bar FIP, HC emissions are lowered by 3.85% when SOI is advanced from 24.5° to 26 °CA bTDC. Nonetheless, advancing the SOI further to 27.5 °CA bTDC increases HC emissions by about 2%. A similar trend is observed for CO emission.
- At 18.5 CR and 26 °CA bTDC SOI, HC emissions are reduced by 7.4% when the FIP is varied from 220 to 240 bar. However, a further increase of the FIP to 260 bar increases HC emissions by about 2%. A similar pattern observed with CO emissions.
- The minimum HC, CO, and smoke emissions are 0.079 g/kWh, 1.9 g/kWh and 26.9% respectively at 18.5 CR, 240 bar FIP, and 26 °CA bTDC SOI.
- The best BTE condition is obtained with maximum peak cylinder pressure and maximum HRR; the emissions (CO, HC and Smoke) are observed to be at their minimum level. Based on this, the engine operating conditions of 18.5 CR, 240 bar FIP, and 26 °CA bTDC SOI to be optimal.
- The HHO + JME20 dual-fuel operation shows higher NO emissions in comparison with baseline data irrespective of the engine condition. The maximum NO emission is observed to be 7.5 g/kWh at 18.5 CR, 220 bar FIP and 26 °CA bTDC SOI which is higher than neat diesel by 34%.

Future scope

The optimized LHR engine operating conditions for running the test diesel engine on HHO + JME20 are 18.5 CR, 240 bar FIP, and 26 °CA bTDC SOI, which are well suited suitable for low-capacity single-cylinder engines. However, the HHO + JME20 operation needs to be optimized for high-capacity multi-cylinder LHR engines. The higher NO emissions need to be regulated by using any of the post or pre-treatment NO mitigation techniques. A few examples of the post-treatment NO mitigation techniques are lean NO_x trap (LNT), selective catalytic reduction (SCR), and SCR filter (SCRf) while examples of pre-treatment NO mitigation techniques are exhaust gas recirculation (EGR), water injection, and doping of additives (nano, antioxidant additives).

Declaration of Competing Interest

The authors declare that they have no known competing financial interests or personal relationships that could have appeared to influence the work reported in this paper.

Data availability

No data was used for the research described in the article.

References

- [1] <https://ourworldindata.org/fossil-fuels>, 2019.
- [2] P. Muñoz, E.A. Franceschini, D. Levitan, C.R. Rodriguez, T. Humana, Perelmuter G. Correa, Comparative analysis of cost, emissions and fuel consumption of diesel, natural gas, electric and hydrogen urban buses, *Energy Convers. Manag.* 257 (2022), 115412, <https://doi.org/10.1016/J.ENCONMAN.2022.115412>.
- [3] <https://www.verifiedmarketresearch.com/product/diesel-engine-market/>, Feb 2020..
- [4] A. Zare, T.A. Bodisco, M.N. Nabi, F.M. Hossain, Z.D. Ristovski, R.J. Brown, Engine performance during transient and steady-state operation with oxygenated fuels, *Energy Fuel* 31 (2017) 7510–7522, <https://doi.org/10.1021/acs.energyfuels.7b00429>.
- [5] S.M.A. Rahman, T.C. Van, F.M. Hossain, M. Jafari, A. Dowell, M.A. Islam, et al., Fuel properties and emission characteristics of essential oil blends in a compression ignition engine, *Fuel* 238 (2019) 440–453, <https://doi.org/10.1016/J.FUEL.2018.10.136>.
- [6] G.A. Karim, *Dual-Fuel Diesel Engines*, CRC PRESS, 2021.
- [7] <https://www.iea.org/reports/global-hydrogen-review-2021/executive-summary>, 2021.
- [8] X. Wang, C. Zhang, W. Gao, Risk assessment of hydrogen leakage in diesel hydrogenation process, *Int. J. Hydrog. Energy* 47 (2022) 6955–6964, <https://doi.org/10.1016/J.IJHYDENE.2021.12.027>.
- [9] T.M. Ismail, K. Ramzy, M.N. Abelwhab, B.E. Elnaghi, M. Abd El-Salam, M.I. Ismail, Performance of hybrid compression ignition engine using hydroxy (HHO) from dry cell, *Energy Convers. Manag.* 155 (2018) 287–300, <https://doi.org/10.1016/J.ENCONMAN.2017.10.076>.
- [10] Brown, Welding, United States Patent. US4014777A, 1977.
- [11] J. Paparao, S. Murugan, Oxy-hydrogen gas as an alternative fuel for heat and power generation applications - A review, *Int. J. Hydrog. Energy* 46 (2021) 37705–37735, <https://doi.org/10.1016/j.ijhydene.2021.09.069>.
- [12] N. Kamaraj, A.K. Subburaj, R.K. Mohanraj, S. Rasu, Experimental investigation on performance, combustion and emission characteristics of CI engine with on-site hydrogen generation, *Mater. Today Proc.* 46 (2020) 5469–5474, <https://doi.org/10.1016/j.matpr.2020.09.199>.
- [13] S. Thangaraj, N. Govindan, Investigating the pros and cons of browns gas and varying EGR on combustion, performance, and emission characteristics of diesel engine, *Environ. Sci. Pollut. Res.* 25 (2018) 422–435, <https://doi.org/10.1007/S11356-017-0369-4>.
- [14] S.K. Pathak, A. Nayyar, V. Goel, Optimization of EGR effects on performance and emission parameters of a dual fuel (Diesel + CNG) CI engine: an experimental investigation, *Fuel* 291 (2021), 120183, <https://doi.org/10.1016/J.FUEL.2021.120183>.
- [15] D. Mendoza-Casseres, G. Valencia-Ochoa, J. Duarte-Forero, Experimental assessment of combustion performance in low-displacement stationary engines operating with biodiesel blends and hydroxy, *Therm. Sci. Eng. Prog.* 23 (2021), 100883, <https://doi.org/10.1016/J.TSEP.2021.100883>.
- [16] M.A. Rahman, Effect of induction hydroxy and hydrogen along with algal biodiesel blend in a CI engine: a comparison of performance and emission characteristics, *Environ. Sci. Pollut. Res.* 26 (2019) 9552–9560, <https://doi.org/10.1007/s11356-019-04380-2>.
- [17] M.K. Baltacioglu, R. Kenanoglu, K. Aydin, HHO enrichment of bio-diesohol fuel blends in a single cylinder diesel engine, *Int. J. Hydrog. Energy* 44 (2019) 18993–19004, <https://doi.org/10.1016/j.ijhydene.2019.02.060>.
- [18] B. Najafi, F. Haghighatshoar, S. Ardabili, S. Band, Chau K. Wing, A. Mosavi, Effects of low-level hydroxy as a gaseous additive on performance and emission characteristics of a dual fuel diesel engine fueled by diesel/biodiesel blends, *Eng. Appl. Comput. Fluid Mech.* 15 (2021) 236–250, <https://doi.org/10.1080/19942060.2021.1871960>.
- [19] D. Sekar, G. Venkadesan, M.S. Panithasan, Optimisation of dry cell electrolyser and hydroxy gas production to utilise in a diesel engine operated with blends of orange peel oil in dual-fuel mode, *Int. J. Hydrog. Energy* 47 (2022) 4136–4154, <https://doi.org/10.1016/j.ijhydene.2021.11.052>.
- [20] F.M. Hossain, M. Nurun Nabi, R.J. Brown, Investigation of diesel engine performance and exhaust emissions of microalgae fuel components in a turbocharged diesel engine, *Energy Convers. Manag.* 186 (2019) 220–228, <https://doi.org/10.1016/J.ENCONMAN.2019.02.061>.
- [21] M.R. Islam, M.N. Nabi, M.N. Islam, The fuel properties of pyrolytic oils derived from carbonaceous solid wastes in Bangladesh, *J. Teknol.* 38 (2003) 75–89, <https://doi.org/10.11113/jt.v38.484>.
- [22] M.N. Nabi, M.G. Rasul, S.M.A. Rahman, A. Dowell, Z.D. Ristovski, R.J. Brown, Study of performance, combustion and emission characteristics of a common rail diesel engine with tea tree oil-diglyme blends, *Energy* 180 (2019) 216–228, <https://doi.org/10.1016/J.ENERGY.2019.05.070>.
- [23] M.N. Nabi, A. Zare, F.M. Hossain, T.A. Bodisco, Z.D. Ristovski, R.J. Brown, A parametric study on engine performance and emissions with neat diesel and diesel-butanol blends in the 13-Mode European Stationary Cycle, *Energy Convers. Manag.* 148 (2017) 251–259, <https://doi.org/10.1016/J.ENCONMAN.2017.06.001>.
- [24] B.J. Mitchell, A. Zare, T.A. Bodisco, M.N. Nabi, F.M. Hossain, Z.D. Ristovski, et al., Engine blow-by with oxygenated fuels: A comparative study into cold and hot start operation, *Energy* 140 (2017) 612–624, <https://doi.org/10.1016/J.ENERGY.2017.08.115>.
- [25] D. Barik, S. Murugan, Experimental investigation on the behavior of a DI diesel engine fueled with raw biogas–diesel dual fuel at different injection timing, *J. Energy Inst.* 89 (2016) 373–388, <https://doi.org/10.1016/j.joei.2015.03.002>.
- [26] B.A. Oni, S.E. Sanni, A.J. Ibegbu, A.A. Adujo, Experimental optimization of engine performance of a dual-fuel compression-ignition engine operating on hydrogen-compressed natural gas and Moringa biodiesel, *Energy Rep.* 7 (2021) 607–619, <https://doi.org/10.1016/j.egy.2021.01.019>.
- [27] E. Büyükkaya, T. Engin, M. Cerit, Effects of thermal barrier coating on gas emissions and performance of a LHR engine with different injection timings and valve adjustments, *Energy Convers. Manag.* 47 (2006) 1298–1310, <https://doi.org/10.1016/J.ENCONMAN.2005.06.021>.

- [28] S. Sodeoka, M. Suzuki, K. Ueno, H. Sakuramoto, T. Shibata, M. Ando, Thermal and mechanical properties of ZrO₂-CeO₂ plasma-sprayed coatings, *J. Therm. Spray Technol.* 6 (1997) 361–367, <https://doi.org/10.1007/s11666-997-0071-z>.
- [29] C.T. Officer, G. Cotton, Greaves Cotton Launches BS- VI Compliant, *World's Cleanest Single Cylinder Diesel Engine*, 2019, 2019–21.
- [30] C. Patel, K. Chandra, J. Hwang, R.A. Agarwal, N. Gupta, C. Bae, et al., Comparative compression ignition engine performance, combustion, and emission characteristics, and trace metals in particulates from Waste cooking oil, *Jatropha* and *Karanja* oil derived biodiesels, *Fuel* 236 (2019) 1366–1376, <https://doi.org/10.1016/j.fuel.2018.08.137>.
- [31] S. Kanth, T. Ananad, S. Debbarma, B. Das, Effect of fuel opening injection pressure and injection timing of hydrogen enriched rice bran biodiesel fuelled in CI engine, *Int. J. Hydrog. Energy* 46 (2021) 28789–28800, <https://doi.org/10.1016/j.ijhydene.2021.06.087>.
- [32] B. Subramanian, V. Thangavel, Experimental investigations on performance, emission and combustion characteristics of Diesel-Hydrogen and Diesel-HHO gas in a dual fuel CI engine, *Int. J. Hydrog. Energy* 45 (2020) 25479–25492, <https://doi.org/10.1016/j.ijhydene.2020.06.280>.
- [33] J.P. Holman, *Experimental Methods for Engineers*, 2012.
- [34] S. Gopinath, P.K. Devan, V. Sabarish, B.V. Sabharish Babu, S. Sakthivel, P. Vignesh, Effect of spray characteristics influences combustion in DI diesel engine - A review, *Mater. Today Proc.* 33 (2020) 52–65, <https://doi.org/10.1016/j.matpr.2020.03.130>.
- [35] A.K. Agarwal, S. Som, P.C. Shukla, H. Goyal, D. Longman, In-nozzle flow and spray characteristics for mineral diesel, *Karanja*, and *Jatropha* biodiesels, *Appl. Energy* 156 (2015) 138–148, <https://doi.org/10.1016/j.apenergy.2015.07.003>.
- [36] S. Lee, C.S. Lee, S. Park, J.G. Gupta, R.K. Maurya, A.K. Agarwal, Spray characteristics, engine performance and emissions analysis for *Karanja* biodiesel and its blends, *Energy* 119 (2017) 138–151, <https://doi.org/10.1016/j.energy.2016.12.043>.
- [37] S. Lahane, K.A. Subramanian, Effect of different percentages of biodiesel-diesel blends on injection, spray, combustion, performance, and emission characteristics of a diesel engine, *Fuel* 139 (2015) 537–545, <https://doi.org/10.1016/j.fuel.2014.09.036>.
- [38] H. Hiroyasu, M. Arai, M. Tabata, Empirical equations for the sauter mean diameter of a diesel spray, *SAE Tech. Pap.* 98 (1989) 868–877, <https://doi.org/10.4271/890464>.
- [39] O.A. Kuti, K. Nishida, J. Zhu, Experimental studies on spray and gas entrainment characteristics of biodiesel fuel: Implications of gas entrained and fuel oxygen content on soot formation, *Energy* 57 (2013) 434–442, <https://doi.org/10.1016/j.energy.2013.05.006>.
- [40] A. Rimkus, J. Matijosić, M. Bogdevičius, Á. Bereczky, Á. Török, An investigation of the efficiency of using O₂ and H₂ (hydroxile gas -HHO) gas additives in a CI engine operating on diesel fuel and biodiesel, *Energy* 152 (2018) 640–651, <https://doi.org/10.1016/j.energy.2018.03.087>.
- [41] V. Chintala, K.A. Subramanian, Experimental investigations on effect of different compression ratios on enhancement of maximum hydrogen energy share in a compression ignition engine under dual-fuel mode, *Energy* 87 (2015) 448–462, <https://doi.org/10.1016/j.energy.2015.05.014>.
- [42] J.B. Heywood, *Internal Combustion Engine Fundamentals*, McGraw-Hill Education, 2018.
- [43] P. Sharma, A. Dhar, Compression ratio influence on combustion and emissions characteristic of hydrogen diesel dual fuel CI engine: Numerical Study, *Fuel* 222 (2018) 852–858, <https://doi.org/10.1016/j.fuel.2018.02.108>.
- [44] B. Ashok, K. Nanthagopal, R.T.K. Raj, J.P. Bhasker, D.S. Vignesh, Influence of injection timing and exhaust gas recirculation of a *Calophyllum inophyllum* methyl ester fuelled CI engine, *Fuel Process. Technol.* 167 (2017) 18–30, <https://doi.org/10.1016/j.fuproc.2017.06.024>.
- [45] A. Syed, S.A.P. Quadri, G.A.P. Rao, W. Mohd, Experimental investigations on DI (direct injection) diesel engine operated on dual fuel mode with hydrogen and mahua oil methyl ester (MOME) as injected fuels and effects of injection opening pressure, *Appl. Therm. Eng.* 114 (2017) 118–129, <https://doi.org/10.1016/j.applthermaleng.2016.11.152>.
- [46] T. Lakshmanan, G. Nagarajan, Experimental investigation on dual fuel operation of acetylene in a DI diesel engine, *Fuel Process. Technol.* 91 (2010) 496–503, <https://doi.org/10.1016/j.fuproc.2009.12.010>.
- [47] J. Papparao, K. Kumar Pandey, S. Murugan, Experimental studies on the effect of TBC piston in a dual-fueled diesel engine, *Fuel* (2021), <https://doi.org/10.1016/j.fuel.2021.121700>.
- [48] J. Hirakude, A.S. Padalkar, Experimental investigation of the effect of compression ratio on performance and emissions of CI engine operated with waste fried oil methyl ester blend, *Fuel Process. Technol.* 128 (2014) 367–375, <https://doi.org/10.1016/j.fuproc.2014.07.026>.
- [49] A.K. Agarwal, A. Dhar, J.G. Gupta, Kim W. Il, K. Choi, C.S. Lee, et al., Effect of fuel injection pressure and injection timing of *Karanja* biodiesel blends on fuel spray, engine performance, emissions and combustion characteristics, *Energy Convers. Manag.* 91 (2015) 302–314, <https://doi.org/10.1016/j.enconman.2014.12.004>.
- [50] M. Akcay, I.T. Yilmaz, A. Feyzioglu, The influence of hydrogen addition on the combustion characteristics of a common-rail CI engine fueled with waste cooking oil biodiesel/diesel blends, *Fuel Process. Technol.* 223 (2021), 106999, <https://doi.org/10.1016/j.fuproc.2021.106999>.
- [51] R.D. Gorle, D.B. Meshram, P.L. Naik, V.S. Narnaware, Optimization of Effective Parameter of *Jatropha* Biodiesel Using Taguchi Method and Performance Analysis Using CI Engine, 2013.
- [52] A.K. Agarwal, A. Dhar, J.G. Gupta, Kim W. Il, C.S. Lee, S. Park, Effect of fuel injection pressure and injection timing on spray characteristics and particulate size-number distribution in a biodiesel fuelled common rail direct injection diesel engine, *Appl. Energy* 130 (2014) 212–221, <https://doi.org/10.1016/j.apenergy.2014.05.041>.
- [53] M.J. Abedin, H.H. Masjuki, M.A. Kalam, A. Sanjid, A.M. Ashraf, Combustion, performance, and emission characteristics of low heat rejection engine operating on various biodiesels and vegetable oils, *Energy Convers. Manag.* 85 (2014) 173–189, <https://doi.org/10.1016/j.enconman.2014.05.065>.
- [54] D. Kannan, M.N. Nabi, J.E. Hustad, Influence of ethanol blend addition on Compression Ignition Engine performance and emissions operated with diesel and *Jatropha Methyl Ester*, *SAE Tech. Pap.* (2009) 4970, <https://doi.org/10.4271/2009-01-1808>.
- [55] G.R. Kannan, R. Anand, Experimental evaluation of DI diesel engine operating with diestrol at varying injection pressure and injection timing, *Fuel Process. Technol.* 92 (2011) 2252–2263, <https://doi.org/10.1016/j.fuproc.2011.07.015>.
- [56] N.A. Bhave, M.M. Gupta, S.S. Joshi, Effect of oxy hydrogen gas addition on combustion, performance, and emissions of premixed charge compression ignition engine exhaust gas temperature, *Fuel Process. Technol.* 227 (2022), 107098, <https://doi.org/10.1016/j.fuproc.2021.107098>.
- [57] L. Lešnik, B. Vajda, Z. Žunić, L. Škerget, B. Kegl, The influence of biodiesel fuel on injection characteristics, diesel engine performance, and emission formation, *Appl. Energy* 111 (2013) 558–570, <https://doi.org/10.1016/j.apenergy.2013.05.010>.
- [58] J. Black, P.G. Eastwood, K. Tufail, T. Winstanley, Y. Hardalupas, A.M.K.P. Taylor, Inter-correlations between smoke opacity, Legal Particulate Sampling (LPS) and TEOM, during transient operation of a diesel engine, *SAE Tech. Pap.* (2007) 571–582, <https://doi.org/10.4271/2007-01-2060>.
- [59] A.C. Alkidas, Relationships between smoke measurements and particulate measurements, *SAE Tech. Pap.* (1984), <https://doi.org/10.4271/840412>.
- [60] J. Hirkude, V. Belokar, J. Randhir, Effect of compression ratio, injection pressure and injection timing on performance and smoke emissions of CI engine fuelled with waste fried oil methyl esters - diesel blend, *Mater. Today Proc.* 5 (2018) 1563–1570, <https://doi.org/10.1016/j.matpr.2017.11.247>.
- [61] S.V. Khandal, N.R. Banapurmath, V.N. Gaitonde, Effect of hydrogen fuel flow rate, fuel injection timing and exhaust gas recirculation on the performance of dual fuel engine powered with renewable fuels, *Renew. Energy* 126 (2018) 79–94, <https://doi.org/10.1016/j.renene.2018.01.049>.
- [62] F.M. Hossain, M.N. Nabi, T.J. Rainey, T. Bodisco, M.M. Rahman, K. Suara, et al., Investigation of microalgae HTL fuel effects on diesel engine performance and exhaust emissions using surrogate fuels, *Energy Convers. Manag.* 152 (2017) 186–200, <https://doi.org/10.1016/j.enconman.2017.09.016>.
- [63] M.S. Gad, M.K. El-Fakharany, E.A. Elsharkawy, Effect of HHO gas enrichment on performance and emissions of a diesel engine fueled by biodiesel blend with kerosene additive, *Fuel* 280 (2020), 118632, <https://doi.org/10.1016/j.fuel.2020.118632>.